

UNCLASSIFIED

AD NUMBER
AD003741
NEW LIMITATION CHANGE
TO Approved for public release, distribution unlimited
FROM Distribution authorized to U.S. Gov't. agencies and their contractors; Administrative/Operational Use; FEB 1953. Other requests shall be referred to Office of Naval Research, Arlington, VA.
AUTHORITY
ONR ltr, 26 Oct 1977

THIS PAGE IS UNCLASSIFIED

Reproduced by

Armed Services Technical Information Agen

DOCUMENT SERVICE CENTER

KNOTT BUILDING, DAYTON, 2, OHIO

AD -

3741

UNCLASSIFIED

AD No. 3241
ASTM LIBRARY

CALIFORNIA INSTITUTE OF TECHNOLOGY

DYNAMIC PROPERTIES LABORATORY

Dynamic Stress-Strain Relations

for

Annealed 2S Aluminum

Under Compression Impact

by

J. E. Johnson, D. S. Wood, and D. S. Clark

49

**A REPORT ON RESEARCH CONDUCTED UNDER
CONTRACT WITH THE OFFICE OF NAVAL RESEARCH**

February 1953

34

DYNAMIC STRESS-STRAIN RELATIONS
FOR ANNEALED 2S ALUMINUM
UNDER COMPRESSION IMPACT

By

J. E. Johnson, D. S. Wood, and D. S. Clark

Seventh Technical Report

under

Office of Naval Research
Contract N6onr-24418
Project Designation NR 031-285

California Institute of Technology
Pasadena, California
February 1953

Dynamic Stress-Strain Relations
For Annealed 2S Aluminum
Under Compression Impact

Table of Contents

Abstract.....	iv
Introduction.....	1
Equipment.....	3
Test Procedure and Experimental Results.....	7
Discussion of Results.....	29
Summary.....	38
Appendix.....	39
References.....	48

LIST OF TABLES

<u>Table No.</u>	<u>Title</u>	<u>Page</u>
I	Elastic Wave Velocities and Moduli of Elasticity.	12
II	Results of Compression Impact Tests	13
III	Propagation Distances of Maximum Strains.	35

LIST OF FIGURES

<u>Fig. No.</u>	<u>Title</u>	<u>Page</u>
1	Section Drawing Vertical Impact Machine	4
2	Static Test Specimens	8
3	Static Stress-Strain Relations.	10
4	Impact Stress vs. Particle Velocity	15
5	Impact Stress vs. Maximum Plastic Strain.	16
6	Tracing of a Record of Stress vs. Time, Impact Velocity 98.5 ft/sec, Specimen No. 18A	17
7	Dynamic Stress-Strain Relations	18
8	Stress-Strain Relations Under Moderate Loading Rates. . .	20
9	Lagrange Diagram.	22
10	Stress vs. Time, Impact Stress 13,400 lb/in. ² , Specimen No. 18E.	24
11	Stress vs. Time, Impact Stress 9,500 lb/in. ² , Specimen No. 5D	24
12	Stress vs. Time, Impact Stress 7,500 lb/in. ² , Specimen No. 4D	25
13	Stress vs. Time, Impact Stress 3,850 lb/in. ² , Specimen No. 40B.	25
14	Plastic Strain Distribution, Impact Stress 13,400 lb/in. ² , Specimen No. 18E.	26
15	Plastic Strain Distribution, Impact Stress 9,500 lb/in. ² , Specimen No. 5D	26
16	Plastic Strain Distribution, Impact Stress 7,500 lb/in. ² , Specimen No. 4D	26
17	Strain vs. Time, Impact Velocity 44.7 ft/sec, 0.9 in. from end, Specimen No. 9A	27
18	Strain vs. Time, Impact Velocity 44.7 ft/sec, 1.0 in. from end, Specimen No. 12A.	27
19	Strain vs. Time, Impact Velocity 44.7 ft/sec, 6.0 in. from end, Specimen No. 13A.	28
20	Strain vs. Time, Impact Velocity 69.8 ft/sec, 16.0 in. from end, Specimen No. 24A.	28
21	Derived Dynamic Stress-Strain Curves Which Depend Upon the Final Strain in Relation to Curves Based on $\sigma - v$ and $\sigma - \epsilon_p$ Measurements	33
22	Lagrange Diagram for Stress-Strain Relation up to 5 per cent Strain	34
23	Steps Illustrating Construction of Lagrange Diagram . . .	43

ABSTRACT

This report presents the results of an experimental study of the stress-strain relation of annealed 2S aluminum when subjected to compression impact. Two methods of securing a dynamic stress-strain curve are considered; namely from the measurement of impact stress as a function of maximum plastic strain and impact stress as a function of the impact velocity. The dynamic stress-strain curves obtained by these methods lie considerably above the static curve. The elevation in stress of the dynamic relations above the static relation increases progressively from zero at the elastic limit to about 20 per cent at a strain of 4.5 per cent. However, the two dynamic relations are not coincident which indicates that the behavior of the material cannot be described by a single stress-strain curve for all impact velocities. A family of stress-strain curves which differ slightly from each other and which depend upon the final strain is postulated in order to correlate both sets of data adequately.

INTRODUCTION

The behavior of metals and alloys under dynamic loading conditions has received considerable attention in recent years (1-6)*. It is found that in the plastic range, the stress for a given strain is increased when the rate of loading is increased. Taylor and Whiffin (7, 8) have found that the strengths of annealed copper and steel under impact conditions are increased above the static values. Habib (9) has shown that in compression impact tests on annealed copper, the stress for a given strain is somewhat greater than the static stress at the same strain. The results of an investigation by Clark and Wood (10) indicate that the ultimate tensile strength of all the materials tested is greater under dynamic conditions than under static conditions.

However, the interpretation of many of the previous investigations in terms of elevated stress-strain relations is questionable as pointed out by Clark and Duwez (6) and Lee and Wolf (11). Furthermore, few tests have been performed in which the complete stress-strain relation followed by a material during high-speed dynamic loading could be accurately determined. Kolsky (12) has performed tests on copper and lead in which the stress-strain relation under very high rates of loading was determined. The results indicate that the stress for a given strain at very high loading rates is equal to about twice the stress under static conditions. However, it is difficult to interpret the results of this investigation since the instantaneous distribution of stress in the specimen may not be simple due to the shape of the specimen and possible boundary constraints acting upon it.

The present investigation makes use of an experimental technique which is believed to provide a basis for the interpretation of the measurements obtained in terms of the stress-strain relation of a material under impact conditions with considerably greater assurance than has been heretofore possible. The technique used to accomplish this is as follows: A compression stress is suddenly applied to one end of a long cylindrical specimen by longitudinal impact with an elastic anvil bar of the same

*Numbers in parentheses refer to the references listed at the end of this report.

diameter as the specimen. The stress-time relation at the impact end of the specimen and the plastic strain distribution in the specimen are measured for various known impact velocities. The theory of plastic wave propagation in long, thin bars, developed by von Kármán (13, 14), is used to deduce the stress-strain curve of the material from these measurements and to describe the deformation process in the specimen during impact. In the present paper, this technique is used to determine dynamic stress-strain relations for annealed 2S aluminum.

EQUIPMENT

The compression impact tests were made with the vertical impact machine shown in Fig. 1, which was described in a previous report (15). Briefly, the features of this machine are as follows: A stationary tobironze anvil bar of the same diameter as the specimen is held vertically in a central position between the rails of the machine by means of a guard tube and expendable spacer. An annealed copper cylinder positioned between the lower end of the anvil bar and a fixed base serves to absorb most of the impact energy in the anvil bar by plastic deformation. Since a slight misalignment between the anvil bar and the specimen may occur, the top end of the anvil bar is provided with a 19-inch radius convex spherical surface to prevent initial impact with the corner of the specimen.

When the specimen impacts the anvil bar, a series of compression strains are propagated through the specimen, and an elastic compression wave is propagated through the anvil bar. Thus, any change in stress at the interface between the anvil bar and specimen is propagated through the anvil bar at the elastic wave velocity. The length of the specimen is much less than the length of the anvil bar; hence, the time required for the first reflecting wave from the lower end of the anvil bar to reach the interface is greater than the time required for complete unloading of the interface by the waves in the specimen. Thus, the interface between the anvil bar and specimen is always unloaded by waves reflected from the free end of the specimen; and consequently, all complex reflections from the lower end of the anvil bar need not be considered.

The hammer, which slides on the two vertical rails, is provided with a central hole through which the guard tube may pass. Twenty rubber bands $3/8$ inch thick and one inch wide, attached to the hammer and frame of the machine, serve as a means for accelerating the hammer to the desired impact velocity. The specimen is held centrally in the hammer by means of a lucite shear disk shrunk onto the bar and clamped in the hammer. The shear disk strikes the top of the guard tube just prior to the impact of the specimen on the anvil bar in such a manner that the specimen is released from the shear disk and impacts the anvil bar while it is free from any constraints due to the accelerating mechanism. The hammer continues downward, passing around the guard tube, and is decelerated by means of four vertical friction brakes.

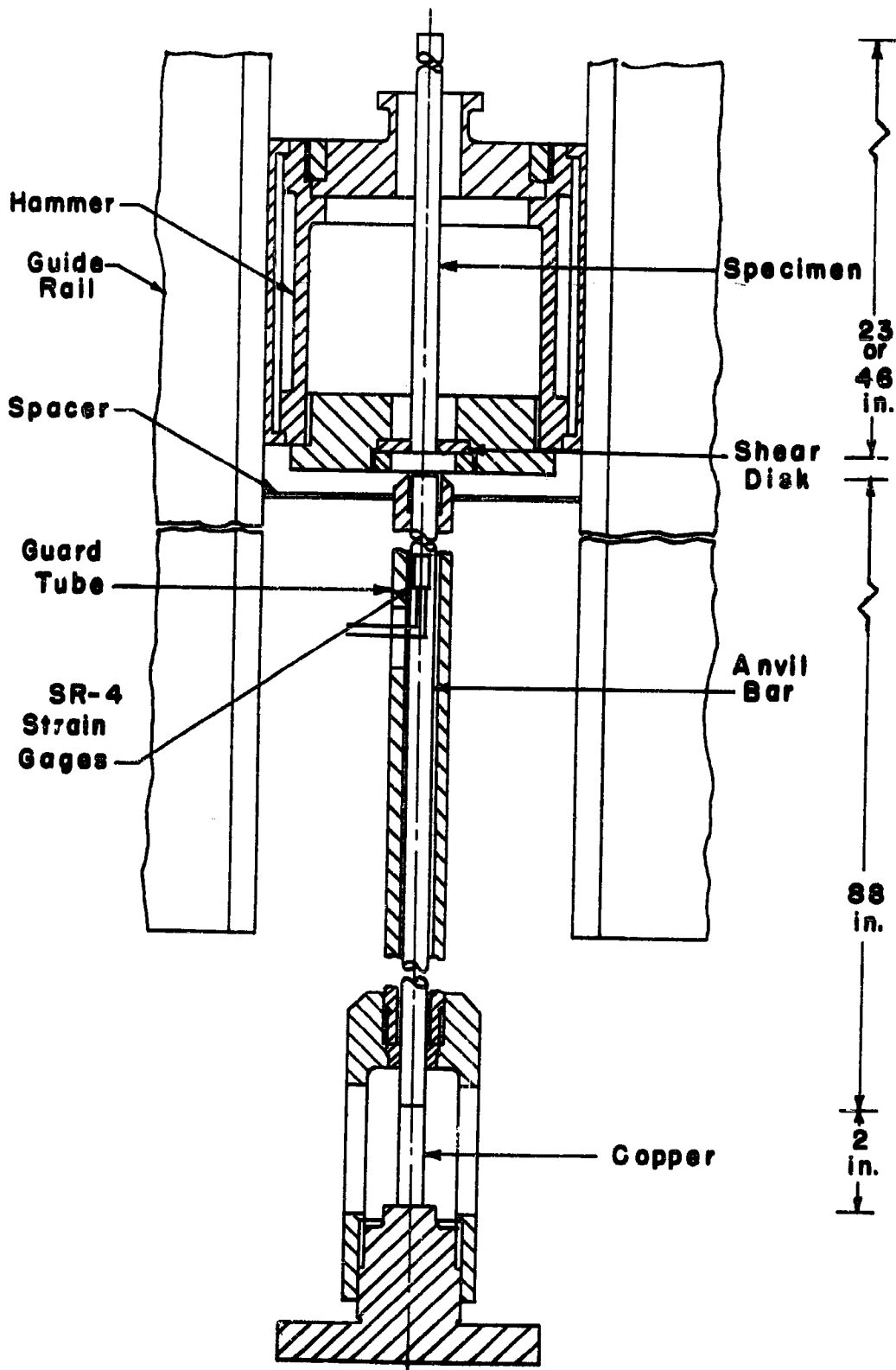


Fig. 1 Section Drawing Vertical Impact Machine

The velocity of the hammer, and, hence, the specimen impact velocity, is determined by measuring the time to travel between three fixed points near the position of impact. This is accomplished by causing electrical contacts to be made at these three points as the hammer passes them, and the signals so produced are recorded on a cathode-ray oscillograph together with an appropriate time calibration trace.

Impact velocities less than 19 ft/sec cannot be accurately determined in the vertical impact machine. For this reason, tests at impact velocities lower than 19 ft/sec were performed by supporting the specimen in a horizontal position as a pendulum by means of six wires attached at two positions along the specimen. The anvil bar was supported in a horizontal position such that the specimen when released from a given height centrally impacted the anvil bar at the minimum point in the swing.

The stress as a function of time at the interface between the anvil bar and specimen is measured during impact by means of SR-4 strain gages cemented to the anvil bar at a position 3 inches from the interface. The strain gages are connected to a suitable recording system employing a single sweep cathode-ray oscilloscope and recording camera. Means for introducing known resistance changes in the strain gage circuit are provided in order to calibrate the stress axis of the records, and appropriate oscillators provide the required time calibrations.

The plastic strain in the specimen after impact is determined with a comparator ruling machine. This machine is used for the purpose of marking the specimen at various intervals along its length with fine scratches before testing and to measure the change in diameter at these positions produced by the impact. The difference between the diameter at any position before and after impact divided by the original diameter is the permanent circumferential plastic strain. The permanent longitudinal plastic strain is equal to twice the circumferential plastic strain since for the maximum strains reached in these experiments (about 5 per cent), no volume changes are produced. This fact was established by static tests in which both circumferential and longitudinal strains were measured.

The comparator ruling machine consists of a sliding carriage which may be accurately positioned along the entire length of a stationary specimen. A scratching device, a low-power microscope, and a diameter

comparator are mounted on the carriage. The scratching device consists of a simple mechanism on which a rigid knife blade is mounted, and this is used to make reference scratches on the specimen. The low-power microscope is equipped with an eyepiece containing cross hairs which permit the accurate positioning of the carriage with respect to any one of the scratches along the specimen. The diameter comparator consists of two knife edges in conjunction with a dial indicator for measuring the diameter of the specimen.

TEST PROCEDURE AND EXPERIMENTAL RESULTS

Preparation of Impact Test Specimens

The specimens used in this investigation were 1/2 in.-diameter extruded 2S aluminum bars. The test specimens were cut from the extruded bars and machined to a length of 23 or 46 in. After machining, the specimens were annealed in a special furnace at 670°F for two hours and furnace-cooled to room temperature. The temperature gradient along the specimen length was less than 12°F.

Static Compression and Tension Tests

Static compression and tension tests were performed in a 150,000 lb Olsen Universal Testing Machine having a least reading of 1 lb (corresponding to a stress of approximately 19 lb/in.² in the gage section of the test specimen). The machine was recently calibrated and showed an error of less than 0.75 per cent. The static compression specimens shown in Fig. 2 were machined from the impact specimens. Eccentric loading was reduced by placing spherical loading blocks at each end of the compression test specimen.

Three tests were performed in which the plastic longitudinal and circumferential strain were measured. A given load was applied to the test specimen and maintained for a period of 20 min or until equilibrium was reached. The load was then removed and the plastic strain in the specimen was measured. The longitudinal strain was determined by measuring the change in the distance between pairs of scratched lines on two opposite sides of the test specimen. This change in distance was determined by means of a filar eyepiece and a low-power microscope. The circumferential strain was determined by measuring the change in diameter of the test specimen. The change in diameter divided by the original diameter is the circumferential plastic strain. The longitudinal plastic strain is the circumferential strain divided by Poisson's ratio which is assumed to be equal to 0.5 for plastic flow. The longitudinal plastic strain could be determined to within 0.0004 in./in. by both methods. A comparison was made between the stress-strain relations obtained by the two methods. The comparison indicates that the stress-strain relations obtained by each method are the same within the accuracy of measurement. The mean stress-strain curve up to 10 per cent strain, corrected for

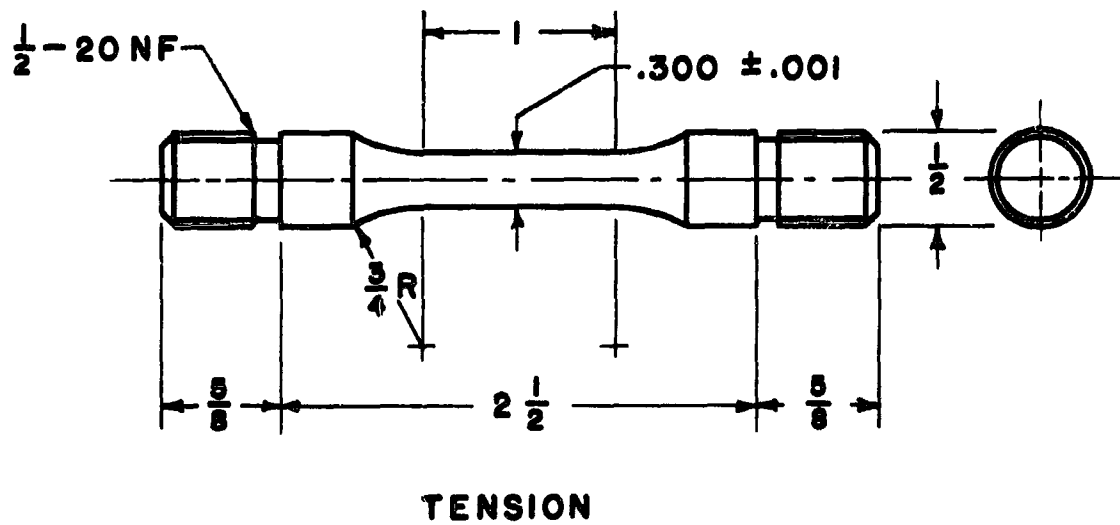
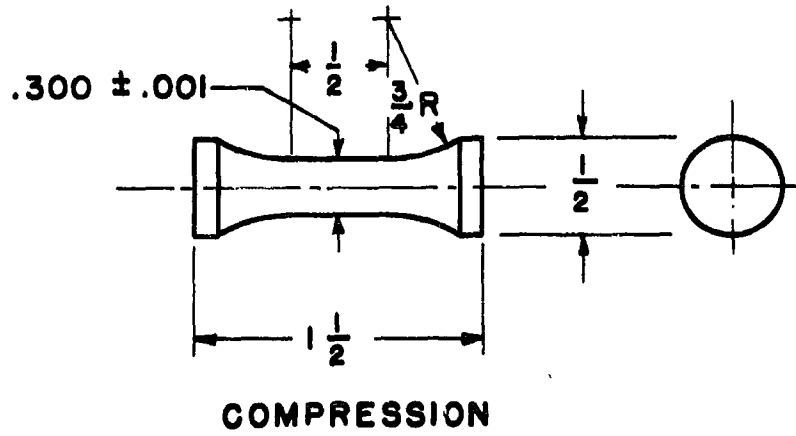


Fig. 2 Static Test Specimens

elastic recovery upon removal of the load, is shown in Fig. 3 by the upper curve denoted "compression."

Two continuous loading static compression tests were performed using SR-4 resistance sensitive wire gages to measure the circumferential strain. The circumferential strain could be determined to within ± 2.3 per cent. The longitudinal strain is determined from the equation

$$\epsilon_L = \frac{-\epsilon_c}{\nu_p} + \frac{\sigma}{E} \left[1 - \frac{\nu_e}{\nu_p} \right] \quad (1)$$

where ϵ_L is the longitudinal strain,
 ϵ_c is the circumferential strain,
 ν_p is Poisson's ratio for plastic flow,
 ν_e is the elastic Poisson's ratio,
 σ is the compressive stress, and
 E is Young's modulus.

The mean static stress-strain curve for the two tests up to 1 per cent strain is shown in Fig. 3 by the lower curve denoted "compression."

Four static tension tests were performed to determine accurately the stress-strain relation at low strain values. The static tension specimen is shown in Fig. 2. The strain in the tension specimen was determined with the use of SR-4 resistance-sensitive wire gages and a Holz extensometer having a least reading of 0.000025 in./in. The mean stress-strain curve for the static tension tests is shown in Fig. 3. The lower curve marked "tension" was obtained with the SR-4 gages, while the upper curve marked "tension" was obtained with the Holz extensometer.

A comparison of the static stress-strain relations obtained by the above methods indicates that for the purpose of this investigation, the longitudinal strain can be accurately determined from circumferential strain measurements.

Determination of the Velocities of Elastic Waves

The velocities of elastic waves in the specimen and in the tobironze anvil bar were determined in order to compute the relations between the strain waves in the specimen and the anvil bar. The elastic wave velocities were determined by measuring the resonance frequency of the bars in longitudinal vibration. The procedure of the previous investigation (15) was followed.

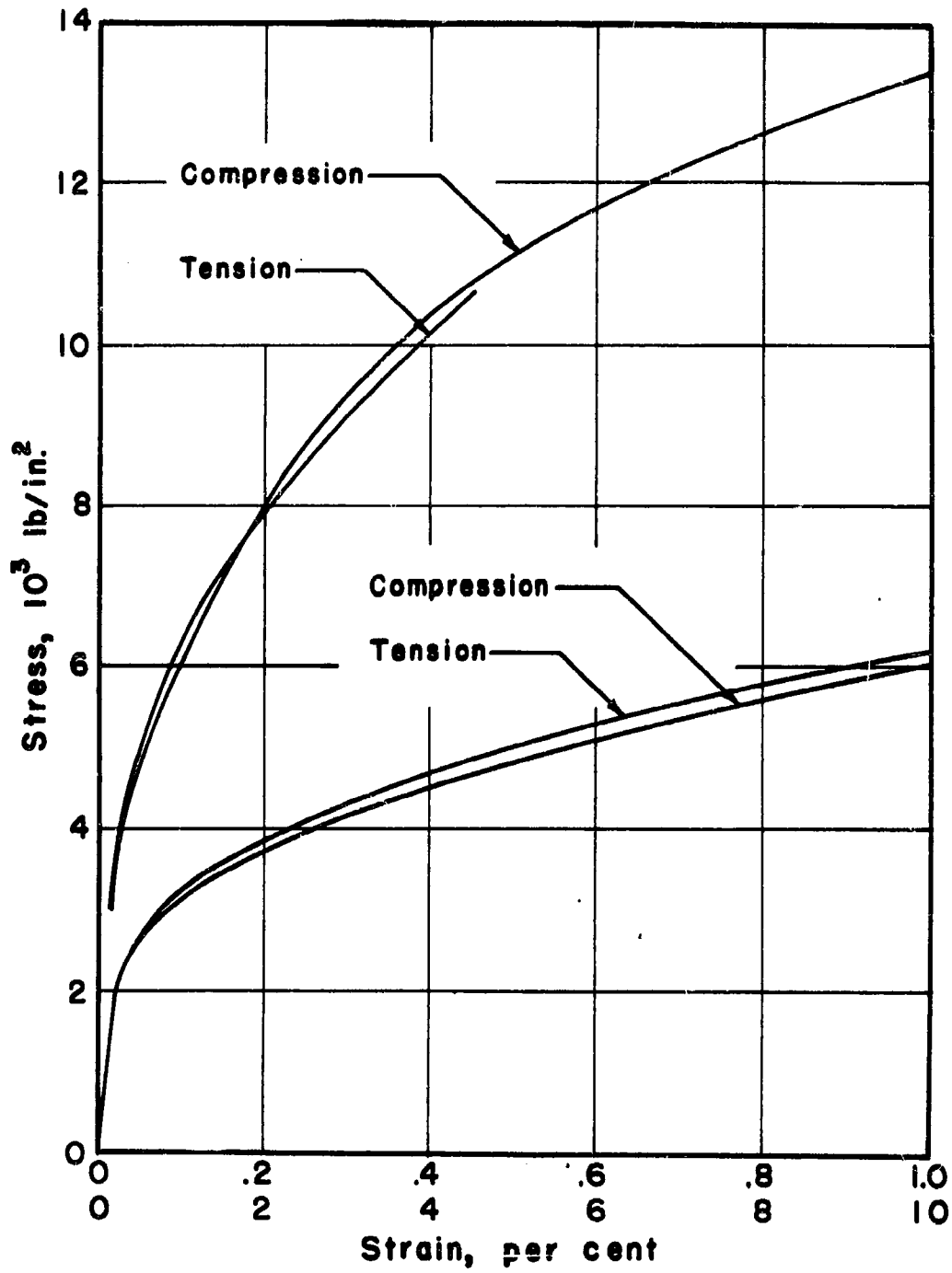


Fig. 3 Static Stress-Strain Relations

The results of the determination of the velocities of propagation of elastic waves for the materials used in this investigation are given in Table I. The resonance frequencies are given for the second and third modes of vibration. The elastic wave velocities are computed for each test, and the average velocity in each material is also given. Young's modulus of each material is computed from the average elastic wave velocity and the mass density, ρ . The value of ρ given for each material in Table I is an average of three densities obtained by weighing a known volume of the material. It is estimated that the accuracy in the determination of elastic wave velocities is within ± 0.6 per cent. The deviation of values of elastic wave velocities from the mean value is less than 0.7 per cent.

Compression Impact Tests

A series of tests was made to determine the relations between the compression stress, σ_1 , at the impact end of the specimen, the plastic strain distribution in the specimen after impact, and the particle velocity, v_1 , imparted to the specimen at the impact end. The particle velocity, v_1 , at the impact end of the specimen differs from the impact velocity, V_0 , since the acoustic impedance of the anvil bar is finite. The particle velocity, v_1 , is given in terms of measured quantities by

$$v_1 = V_0 - \frac{\sigma_1}{\rho_1 c'_0} \quad (2)$$

where V_0 is the velocity of impact,

σ_1 is the compression stress at the interface,

ρ_1 is the mass density of the anvil bar, and

c'_0 is the velocity of propagation of an elastic wave in the anvil bar.

The results of the compression impact tests are summarized in Table II. The plastic strain distribution in the specimen after impact was determined for most of the tests. The maximum plastic strain near the impact end of the specimen for these tests is also given in Table II. Impact velocities from 19.2 to 125 ft/sec were obtained in the vertical impact machine. Impact velocities from 3.15 to 15.9 ft/sec were obtained by supporting the specimen horizontally as a pendulum. The points representing the particle velocity, v_1 , as a function of maximum compression

Table I

ELASTIC WAVE VELOCITIES AND MODULI OF ELASTICITY

<u>Test Number</u>	<u>Length in.</u>	<u>Mode</u>	<u>Resonance Frequency Cycles/sec</u>	<u>Elastic Wave Velocity in./sec</u>	<u>Modulus of Elasticity 10^6 lb/in.²</u>
Determinations on Annealed 2S Aluminum					
$\rho = 2.54 \times 10^{-4}$ lb sec ² /in. ⁴					
1	48	2	4076	195,600	
2	48	2	4062	195,000	
3	48	3	6154	196,900	
4	48	2	4084	196,000	
5	47 31/32	2	4065	195,000	
6	47 31/32	2	4060	194,800	
7	47 31/32	2	4060	194,800	
8	47 31/32	3	6110	<u>195,400</u>	
			Average	195,400	9.71

Determinations on Anvil Bar
(tobin bronze)

$$\rho = 7.85 \times 10^{-4} \text{ lb sec}^2/\text{in.}^4$$

9	87 13/16	2	1587	139,200	
10	87 13/16	2	1589	139,600	
11	87 13/16	3	2387	139,700	
12	87 13/16	3	2391	139,900	
13	87 13/16	2	1585	<u>139,100</u>	
			Average	139,500	15.2

Table II
RESULTS OF COMPRESSION IMPACT TESTS

Specimen Number	Maximum Stress 10^3 lb/in. ²	Velocity of Impact ft/sec	Maximum Particle Velocity ft/sec	Maximum Permanent Strain per cent
20A	1.30	3.15	2.16	--
21C	1.82	4.50	3.12	--
20B	2.43	6.21	4.36	--
20C	2.78	8.00	5.88	--
20D	2.90	9.82	7.61	--
21B	3.23	10.0	7.54	--
40A	3.35	12.4	9.83	--
40B	3.84	14.6	11.6	--
6A	4.12	16.8	13.6	0.30
5A	4.17	16.8	13.6	0.35
21A	4.21	15.9	12.7	--
19F	4.65	19.2	15.7	0.25
5F	5.07	19.7	15.8	0.35
22C	5.23	25.3	21.3	0.45
5E	5.74	26.6	22.2	0.50
22D	5.81	29.9	25.5	0.55
19E	5.87	31.1	26.6	0.70
23A	6.23	33.2	28.5	0.70
19D	6.36	37.6	32.8	0.90
23B	6.68	38.2	33.1	0.90
4E	7.45	43.9	38.2	1.10
4D	7.52	45.8	40.1	1.10
4C	7.56	44.8	39.0	1.10
4B	7.58	44.3	38.5	1.10
4F	7.60	45.4	39.6	1.05
4A	7.65	44.9	39.1	1.10
1A	7.68	44.5	38.6	1.20
1B	8.22	52.0	45.7	1.45
1C	8.82	58.2	51.5	1.65
1D	9.39	67.1	60.0	1.90
5D	9.48	71.6	64.4	2.05
1E	9.94	70.8	63.3	2.20
1F	9.98	76.0	68.4	2.35
35A	10.4	80.0	72.1	2.65
35B	10.6	87.5	79.4	2.85
17E	11.5	97.0	88.3	3.20
18A	11.8	98.5	89.5	3.40
18B	12.2	103	93.9	3.65
19A	12.4	122	113	3.85
18C	12.5	111	102	4.00
18D	12.8	115	106	4.15
18E	13.0	123	113	4.65
18F	13.4	125	115	4.80

stress, σ_1 , at the impact end of the specimen are plotted in Fig. 4. The points representing maximum compression stress, σ_1 , as a function of the measured strain, ϵ_1 , near the impact end of the specimen are plotted in Fig. 5. The strains are corrected for the elastic recovery upon removal of the load. A tracing of a typical record of stress vs. time at the impact end of the specimen is shown in Fig. 6.

The stress-strain relation exhibited by the material may be deduced rather simply from the experimentally determined σ_1 versus v_1 relation if the following assumptions are made. First, it is assumed that the stress-particle velocity relationship during loading follows this curve continuously up to the point corresponding to the given impact stress. As is discussed later, however, this relation may only represent the locus of the terminal points of a number of distinct stress-particle velocity curves which depend upon the impact stress. Second, it is assumed that the kinetic energy and shear stresses associated with the lateral motion of the particles of the specimen can be neglected. The stress-strain relation obtained under these assumptions will later be compared with other experimental results to determine the validity of these assumptions.

Under these assumptions, the strain corresponding to a given stress may be expressed in terms of a definite integral which depends upon the slope of the stress-particle velocity relation up to the given stress. Thus, the strain, $\bar{\epsilon}_1$, at the impact end of the specimen corresponding to a given impact stress, σ_1 , may be expressed in terms of the experimental σ_1 versus v_1 relation by

$$\bar{\epsilon}_1 = \int_0^{\sigma_1} \frac{d\sigma}{\left(\frac{d\sigma}{dv}\right)^2} \quad (3)$$

The slope of the σ_1 versus v_1 curve shown in Fig. 4 is determined at conveniently located points, and the σ_1 versus $\bar{\epsilon}_1$ relation is computed numerically using Equation 3. This stress-strain relation is shown in Fig. 7 by the curve designated as stress-velocity measurements. The static stress-strain curve and the stress-strain relation, σ_1 versus ϵ_1 , determined from impact stress and measured plastic strain are

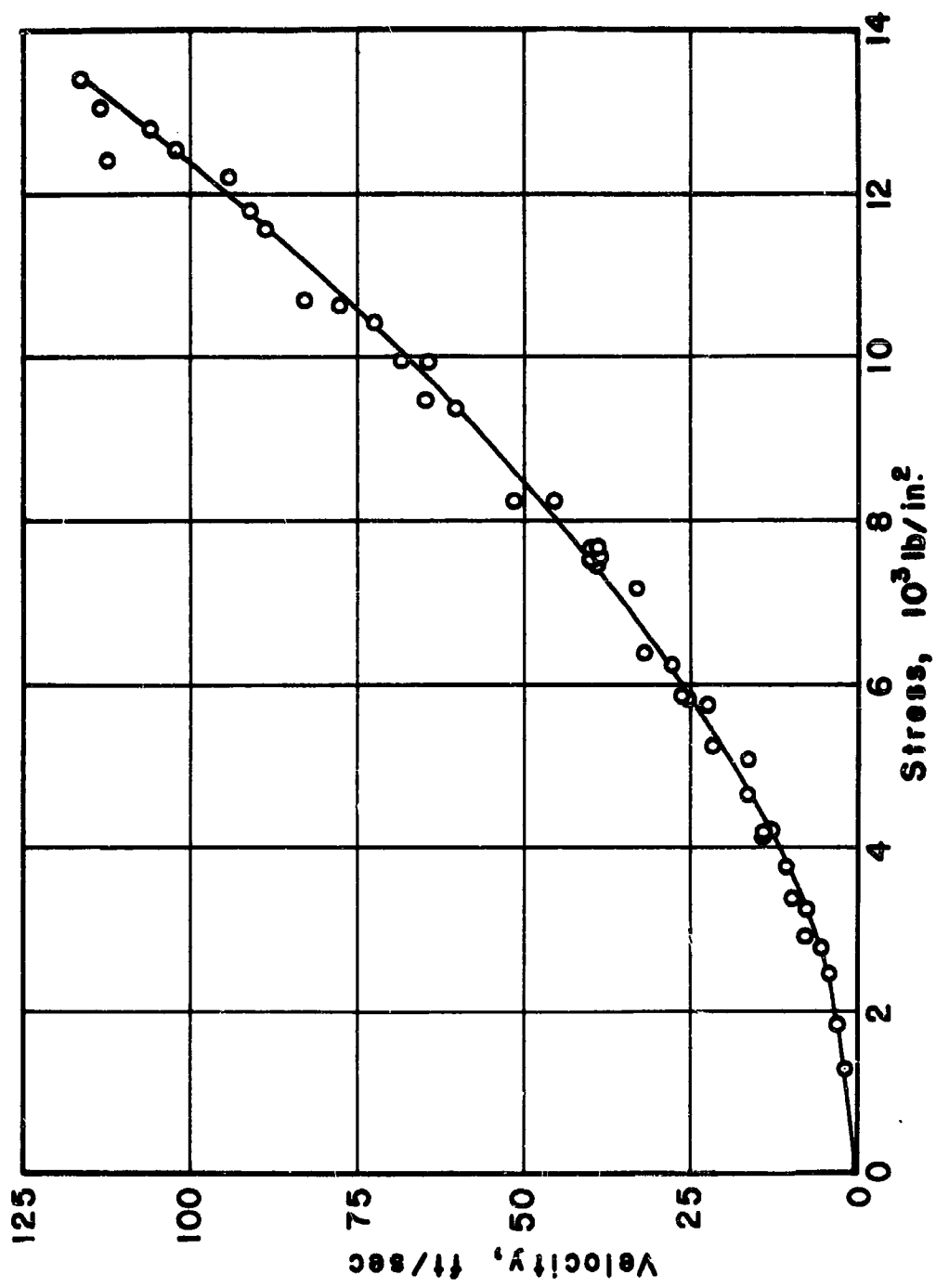


Fig. 4 Impact Stress vs. Particle Velocity

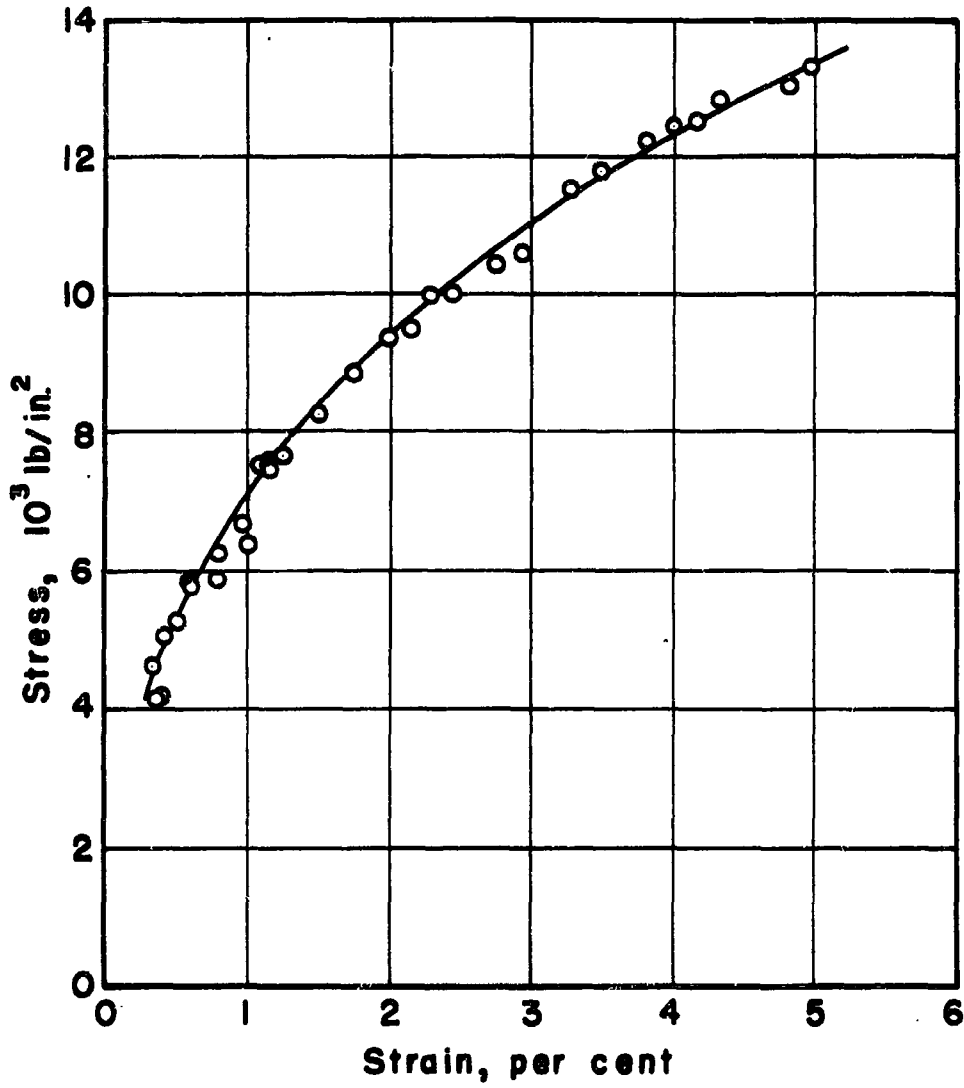


Fig. 5 Impact Stress vs. Maximum Plastic Strain

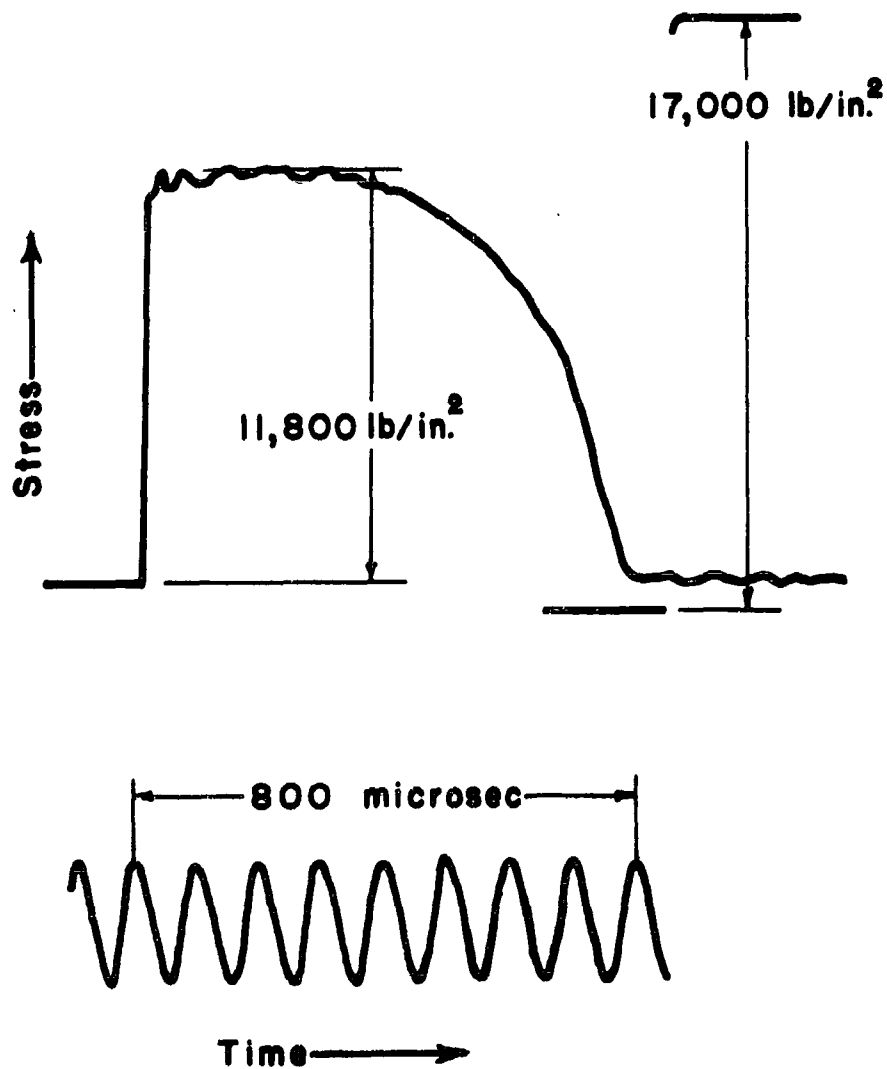


Fig. 6 Tracing of a Record of Stress vs. Time,
Impact Velocity 98.5 ft/sec, Specimen No. 18A

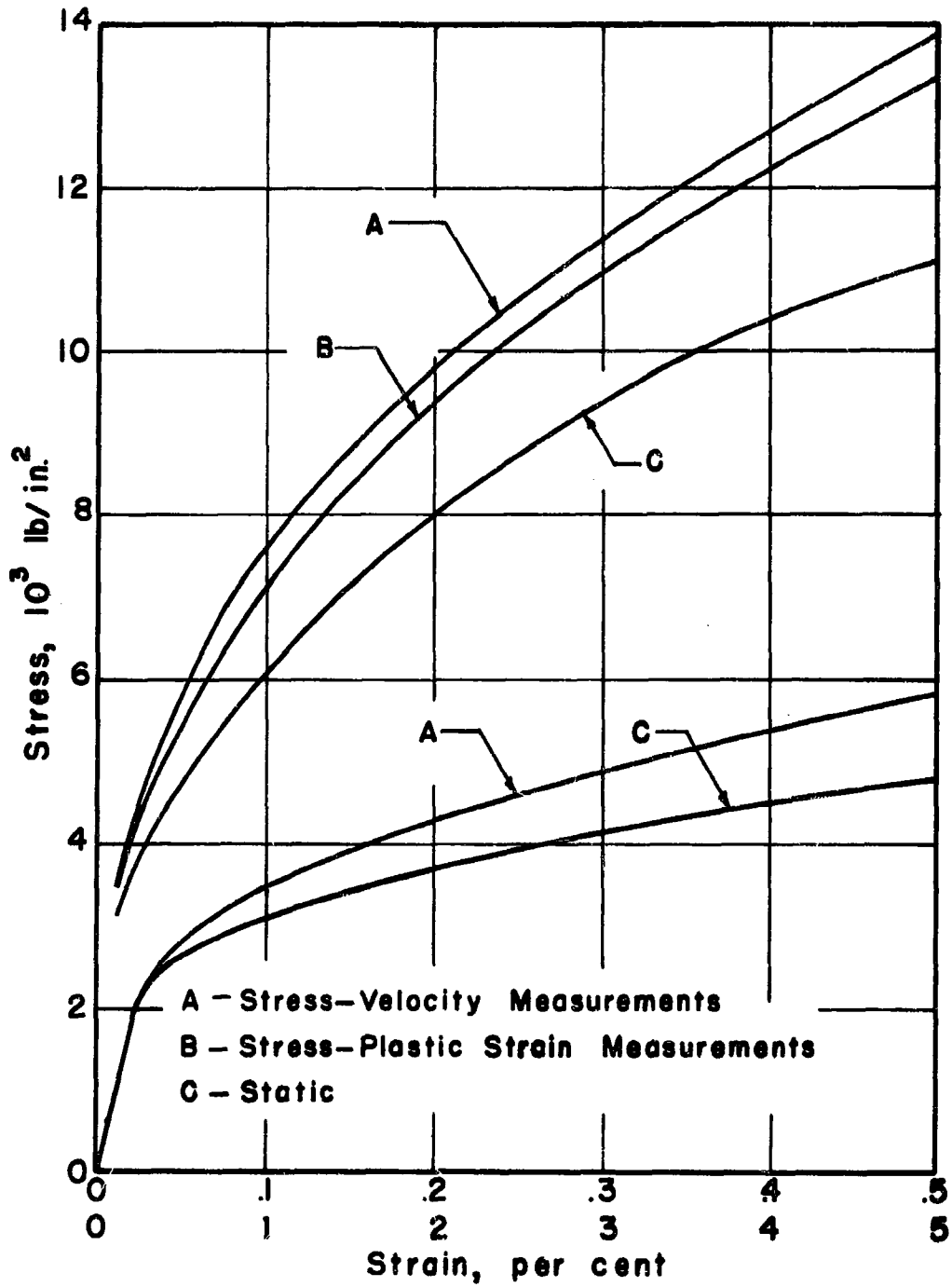


Fig. 7 Dynamic Stress-Strain Relations

shown for comparison. The latter is designated by the curve, stress-plastic strain measurements.

The stress-strain curve deduced from stress-velocity measurements is somewhat different from the curve determined from stress-measured strain. Thus, for a given stress, the strain deduced from stress-velocity measurements with the theory of plastic wave propagation is less than the measured strain after impact. However, both of these stress-strain relations lie considerably above the static stress-strain relation. Thus, the experimental results indicate that under these impact conditions, the excess of the stress at a given strain over the static stress at the same strain increases progressively from zero at the elastic limit to about 20 per cent at a strain of 4.5 per cent.

Moderate Loading Rate Tests

A further series of tests performed at moderate strain-rates indicates that for this material, the relatively large increase in stress for a given strain under impact conditions is associated only with the extremely high loading rates accompanying impact.

The moderate loading rate tests were performed in a rapid-load testing machine by manipulating the load actuating mechanism in such a manner that a nearly constant rate of strain was obtained. The specimens were the same as the static-tension specimens shown in Fig. 2. The load acting on the specimen was measured by means of a dynamometer employing type AB-14, SR-4 strain gages with suitable temperature compensation. The strain in the specimen was measured by means of an extensometer employing similar SR-4 strain gages. The load and the strain were recorded on photographic paper by a recording oscillograph. Timing lines at intervals of 0.1 sec were projected onto the test record to provide a time base. The stress could be determined to within ± 1.5 per cent and the strain to within ± 1 per cent. Two loading rates were used. These loading rates corresponded to strain rates of 0.011/min and 0.040/min. The stress-strain curves for the two rates are shown in Fig. 8, together with the static stress-strain curve. These results show that no significant changes in the stress-strain curve are produced by moderate loading rates.

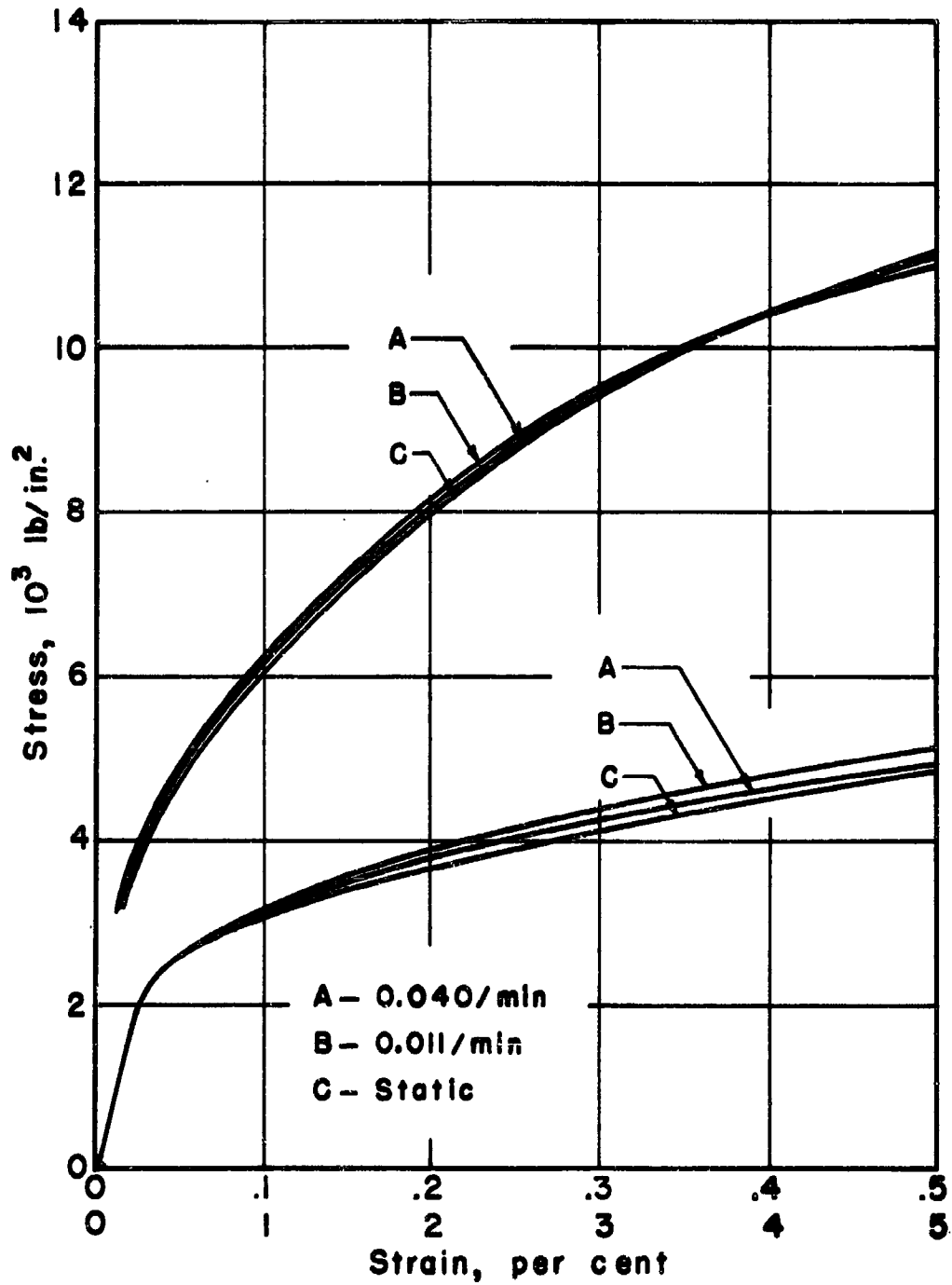


Fig. 8 Stress-Strain Relations Under Moderate Loading Rates

Lagrange Diagram

The process of wave propagation in the specimen can be deduced from a stress-strain relation of the material and represented in a Lagrange or position-time diagram. The stress, strain, and particle velocity are determined as functions of position and time from this diagram. Thus, the stress-time and strain-position relations deduced by means of a Lagrange diagram from the stress-strain relation can be compared with the experimentally determined relations. The dynamic stress-strain curve deduced from maximum stress-impact velocity measurements was used in constructing such a Lagrange diagram. It is assumed that the stress-strain path during loading follows this stress-strain relation and upon unloading follows the normal elastic hysteresis relation. The theory and graphical solutions for strain propagation as developed by von Kármán, Bohnenblust, Hyers, and Charyk (16, 17) were used in constructing the Lagrange diagram shown in Fig. 9. The details of the method of constructing a Lagrange diagram from a stress-strain relation are given in the appendix.

The Lagrange diagram was constructed for the maximum impact stress, $\sigma_1 = 13,400 \text{ lb/in.}^2$, employed in the impact tests. The diagram consists of three regions; namely, a plastic region, an elastic hysteresis region, and the region representing the unloaded state ahead of the initial elastic wave front. The heavy irregular line represents the boundary between the plastic and hysteresis regions for the maximum velocity of impact. The lighter lines indicate the appropriate characteristics in the Lagrangean plane. The diagram includes the portion of the anvil bar on which the strain gages are mounted so that the stress-time relation at the gages may be determined and compared with the experimental measurements. The line, $x = 0$, represents the interface between the specimen and anvil bar. Similar Lagrange diagrams were also constructed for impact stresses of $9,500 \text{ lb/in.}^2$, $7,500 \text{ lb/in.}^2$, and $3,850 \text{ lb/in.}^2$. The plastic hysteresis boundary lines for these cases are indicated in Fig. 9 by the heavy dashed lines, together with those portions of the heavy full line which are common to the several diagrams.

A prediction of the stress as a function of time at the interface between the specimen and anvil bar may be determined from the Lagrange diagram. Such stress-time relations for impact stresses of $13,400 \text{ lb/in.}^2$,

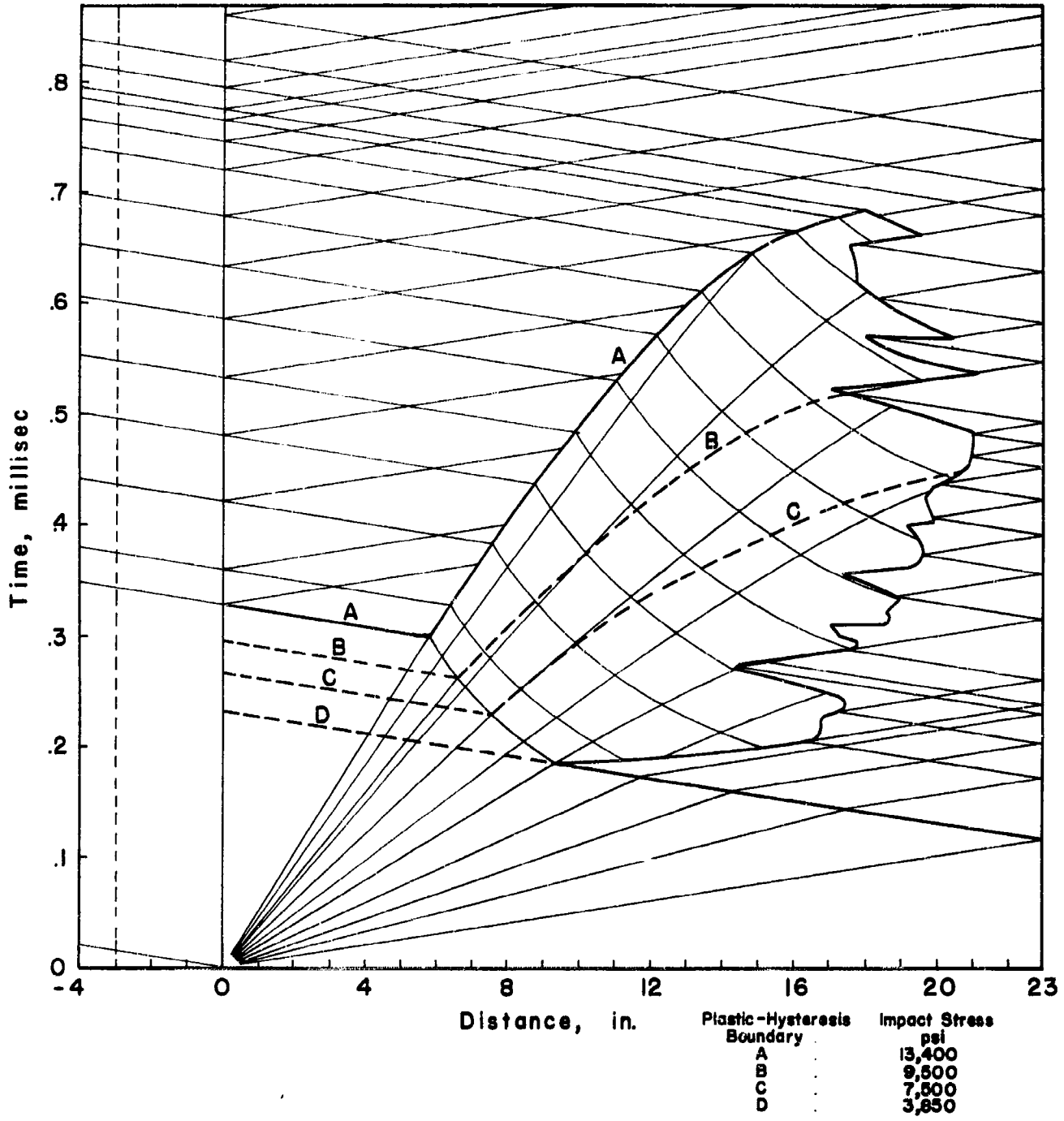


Fig. 9 Lagrange Diagram

9,500 lb/in.², 7,500 lb/in.², and 3,850 lb/in.² are shown in Figs. 10, 11, 12, and 13 respectively, together with the corresponding experimental relations obtained from stress-time measurements. The plastic strain distributions determined from the Lagrange diagram for the first three of the above impact stresses are shown in Figs. 14, 15, and 16, together with the measured strain distributions.

The plastic strain distributions shown in Figs. 14, 15, and 16 indicate that the maximum plastic strains at the impact end of the specimen which are computed from the Lagrange diagram are not equal to the measured strains. The measured plastic strain near the impact end of the specimen is greater than the maximum plastic strain computed from the Lagrange diagram. A comparison of other plastic strain distributions indicates that in nearly every case the measured maximum strain is greater than the computed maximum strain. For this reason, strain as a function of time during impact was determined experimentally at several positions along the bar in an attempt to explain the discrepancy.

The strain in the specimen as a function of time was determined during impact with the use of SR-4 resistance sensitive wire strain gages cemented to the specimen. Gages were mounted in such a manner that the circumferential strain was recorded. In this manner, tension strains are measured. This was considered necessary since the reliability of wire strain gages at large values of compressive strains is uncertain (18). One channel of the recording system was used to determine stress-time at the impact end of the specimen in the usual manner, and the other channel was used for strain-time measurements. A reference timing mark was simultaneously impressed on each oscilloscope screen trace of stress-time and strain-time in order to establish the time at impact on the strain-time record.

Four typical experimental strain-time records are shown in Figs. 17, 18, 19, and 20. The strain-time relations are also determined theoretically from the Lagrange diagram and shown in the figures for comparison. The results indicate that the maximum strain determined from strain-time records near the impact end of the specimen is comparable with the measured strain after impact. Furthermore, this maximum strain is obtained during the initial loading of the specimen, and the strain remains nearly constant after this maximum strain is reached.

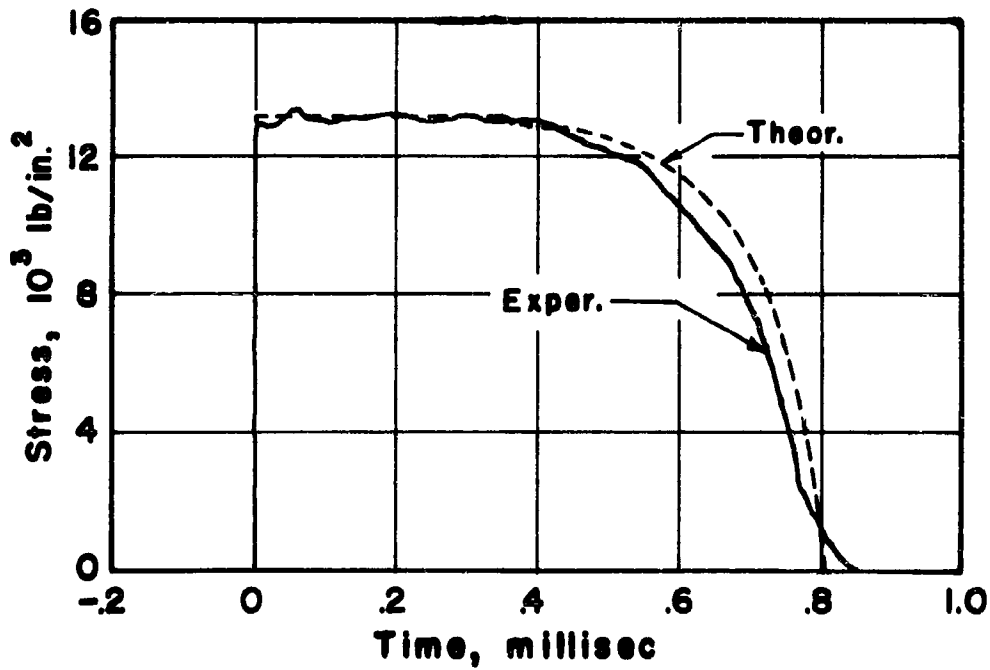


Fig. 10 Stress vs. Time, Impact Stress $13,400 \text{ lb/in.}^2$, Specimen No. 18E

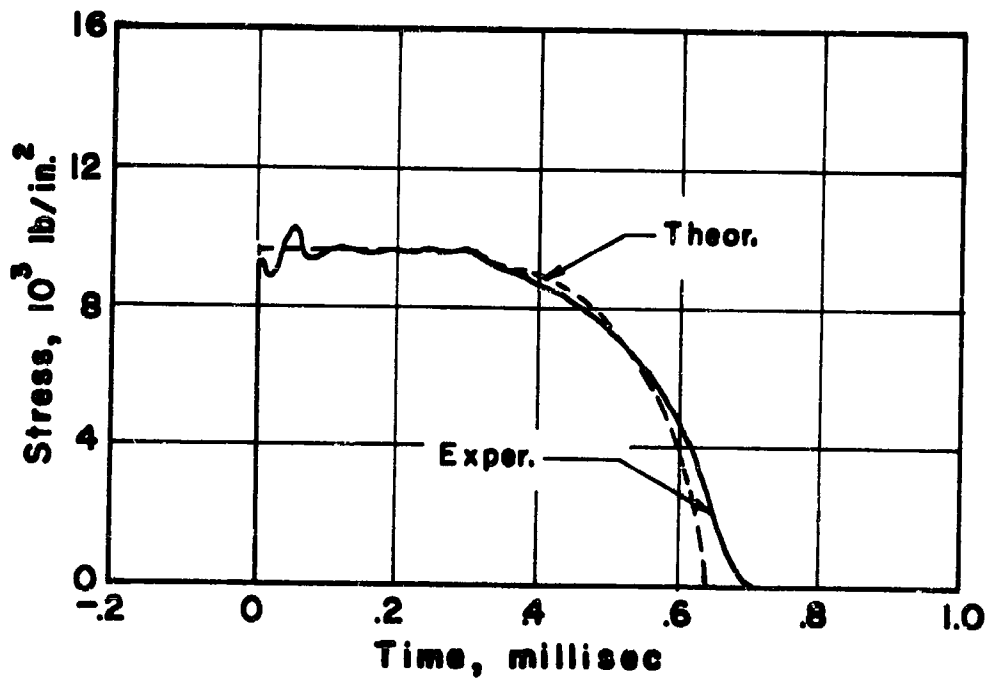


Fig. 11 Stress vs. Time, Impact Stress $9,500 \text{ lb/in.}^2$, Specimen No. 5D

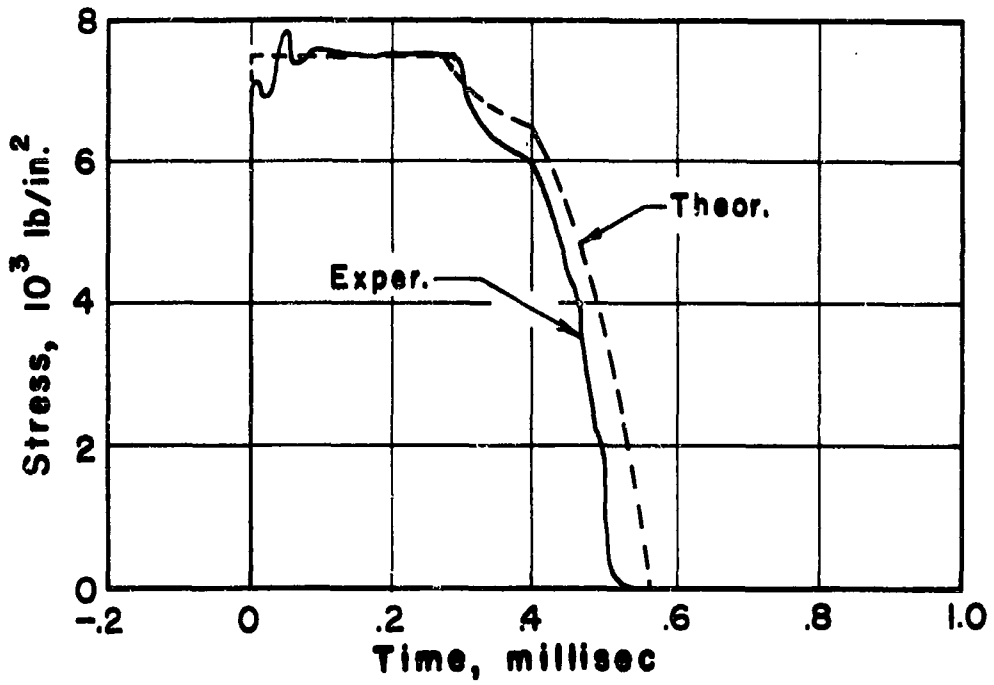


Fig. 12 Stress vs. Time, Impact Stress 7,500 lb/in.², Specimen No. 4D

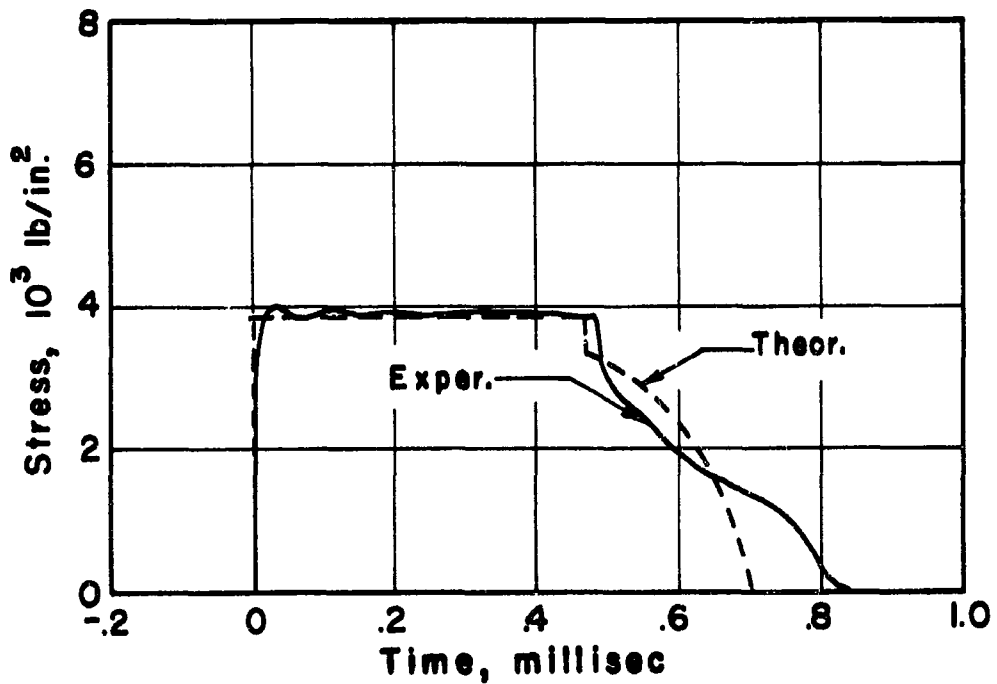


Fig. 13 Stress vs. Time, Impact Stress 3,850 lb/in.², Specimen No. 40B

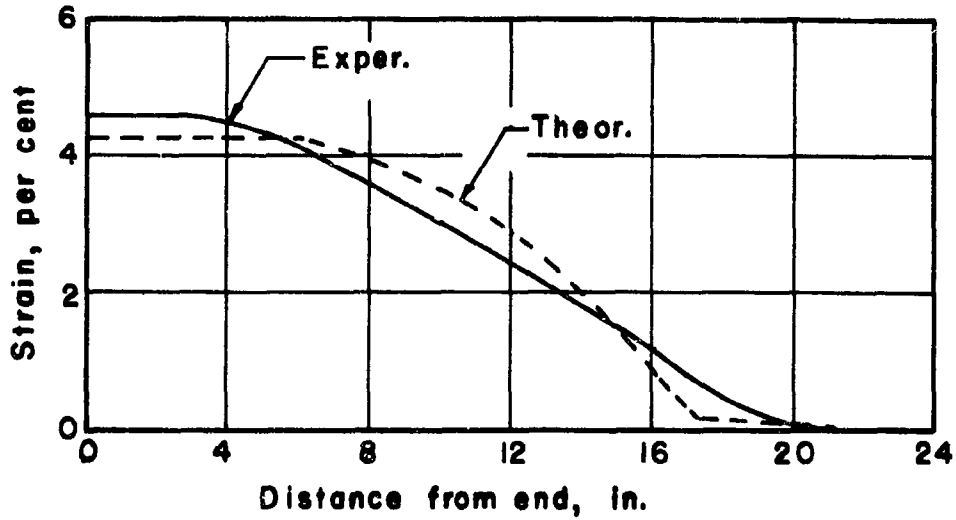


Fig. 14 Plastic Strain Distribution, Impact Stress 13,400 lb/in.², Specimen No. 18E

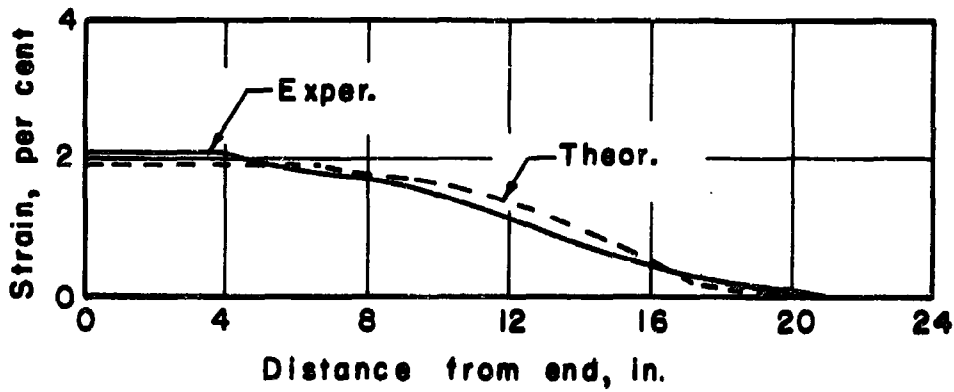


Fig. 15 Plastic Strain Distribution, Impact Stress 9,500 lb/in.², Specimen No. 5D

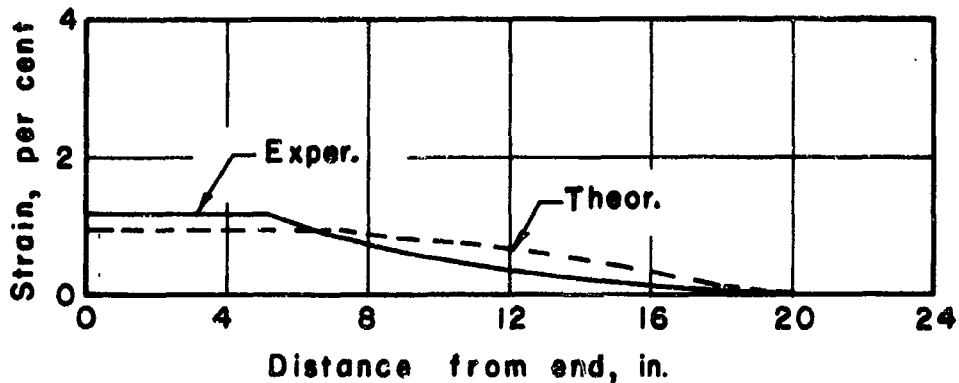


Fig. 16 Plastic Strain Distribution, Impact Stress 7,500 lb/in.², Specimen No. 4D

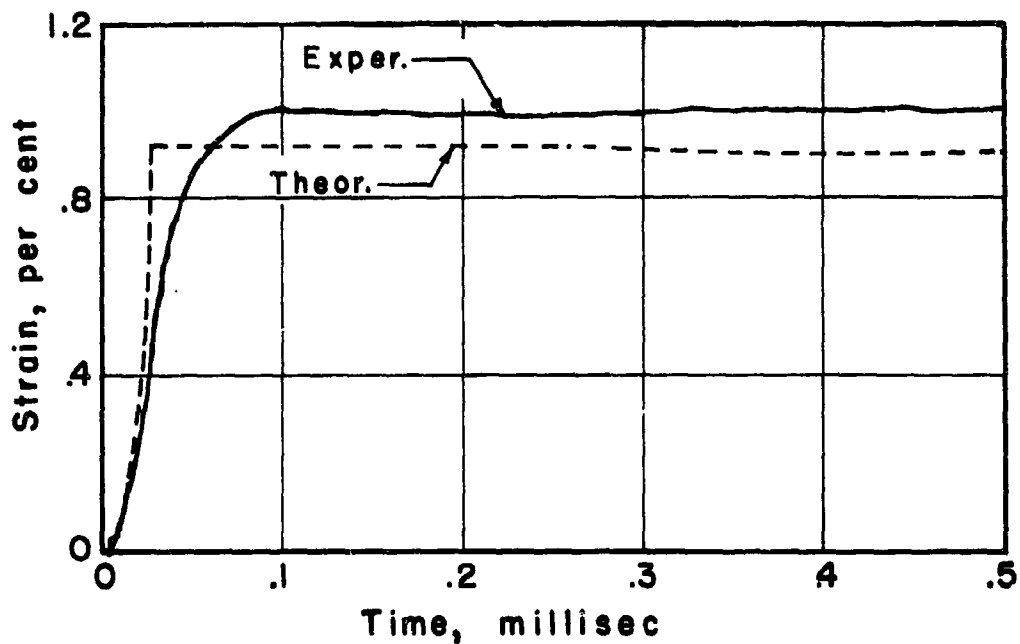


Fig. 17 Strain vs. Time, Impact Velocity 44.7 ft/sec, 0.9 in. from end, Specimen No. 9A

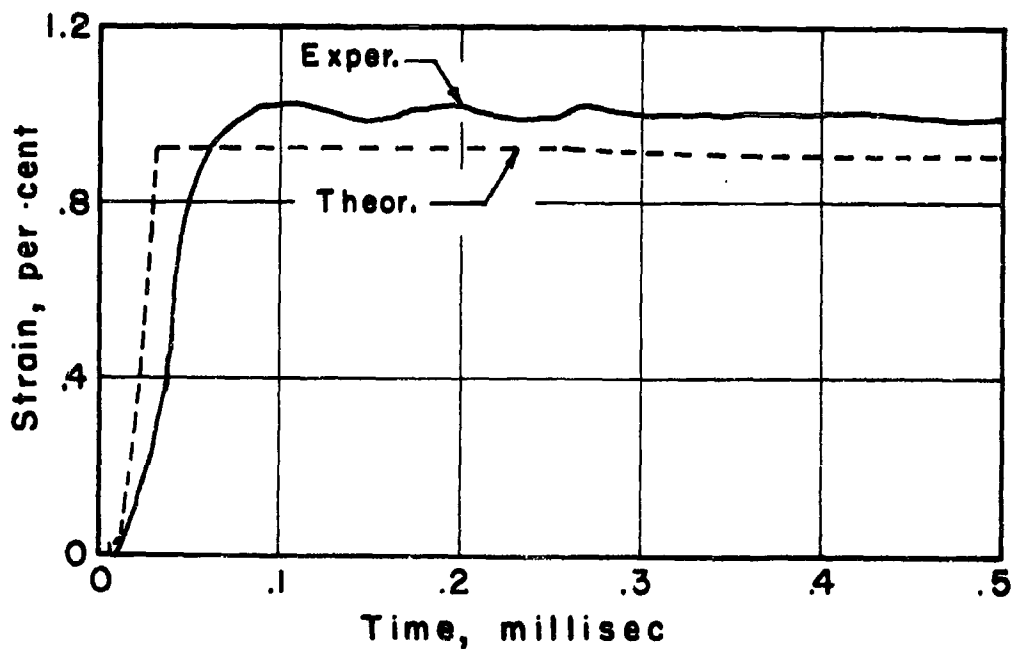


Fig. 18 Strain vs. Time, Impact Velocity, 44.7 ft/sec, 1.0 in. from end, Specimen No. 12A

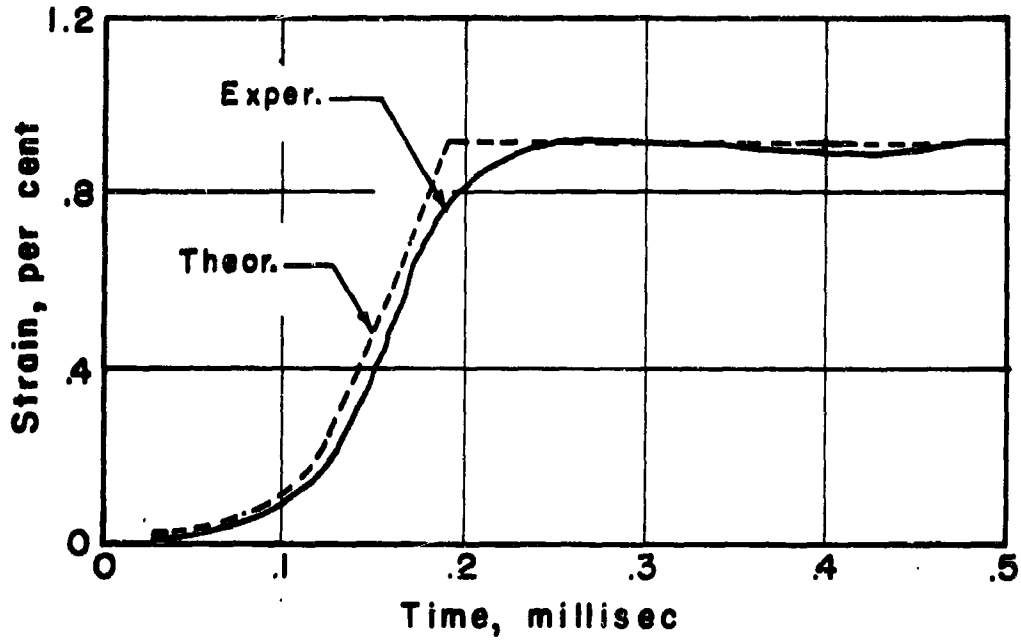


Fig. 19 Strain vs. Time, Impact Velocity 44.7 ft/sec,
6.0 in. from end, Specimen No. 13A

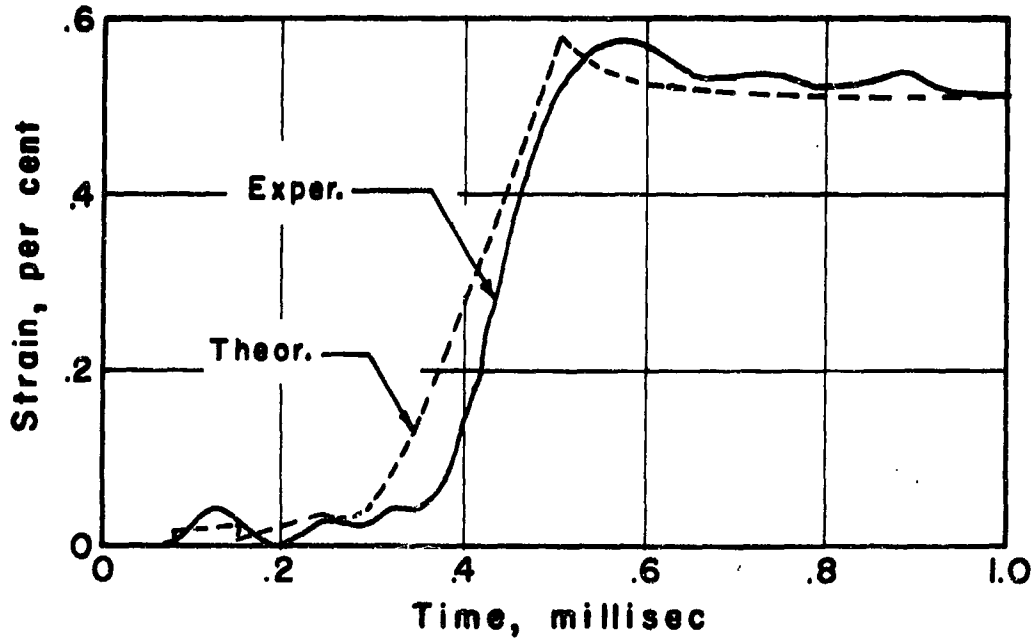


Fig. 20 Strain vs. Time, Impact Velocity 69.8 ft/sec,
16.0 in. from end, Specimen No. 24A

DISCUSSION OF RESULTS

The experimental results of this investigation indicate that the stress-strain relation deduced from stress-velocity measurements with the use of the theory of propagation of plastic strains lies above the stress-strain relation determined from stress-plastic strain measurements. Thus, for a given stress, the strain deduced from stress-velocity measurements is less than the strain measured after impact. However, a dynamic stress-strain relation determined from either stress-velocity measurements or stress-plastic strain measurements lies considerably above the static stress-strain relation.

The dynamic stress-strain relation cannot continue to represent the behavior of the material for an indefinite time, and the stress and strain must approach some equilibrium position on the static stress-strain curve if the load is maintained long enough. Thus, the plastic strain measured after impact may represent the strain associated with the wave propagation process and an additional strain due to relaxation which takes place after the initial impact. The stress-strain relation during relaxation cannot be determined from the experimental data, but the overall magnitude of the maximum strain relaxation compatible with experimental observations can be estimated.

The initiation of any additional plastic strain at the interface between the anvil bar and specimen after initial impact must be accompanied by elastic unloading waves propagating through the specimen and anvil bar. Thus, any increase in strain after the initial strain must be accompanied by a decrease in stress at the interface. However, the experimental stress-time records indicate that during impact the stress at the impact end of the specimen remains nearly constant up to the time at which unloading waves originating from the free end of the specimen arrive. This can be seen in Figs. 10, 11, 12, and 13. Furthermore, any increase in strain which might take place following the passage of the initial strain waves would be expected to produce a nonuniform distribution of permanent strain in the section of the specimen adjacent to the impact end. That this is not the case is illustrated by the typical experimental permanent strain distribution relations shown in Figs. 14, 15, and 16. Furthermore, the strain-time records shown in Figs. 17 and 18 show that the full value of the permanent strain near the impact

end is attained during the passage of the initial plastic wave front. (The rounding over in these records as the strain approaches its maximum value is due to the limited high frequency response characteristics of the amplification system employed and does not represent any real effect in the material.) For these reasons, it may be concluded that no appreciable strain due to relaxation effects has taken place in the period of time during which the impact stress is maintained in these experiments. (This time may be seen from the Lagrange diagram in Fig. 9 to be from about 0.23 to about 0.33 millisecc, depending upon the impact stress) Therefore, some other explanation must be sought to explain the differences between the dynamic stress-strain relations as determined from stress-velocity measurements and from stress-permanent strain measurements.

The desired correlation of the experimental data may be obtained by abandoning the assumption that a single dynamic stress-strain relation exists which is capable of describing the behavior of the material for all impact stresses. A family of stress-strain relations, each member of which depends upon the impact stress, may be used to explain the discrepancy between measured strain and strain values deduced from stress-velocity measurements. Each member of this family of stress-strain relations must satisfy several conditions determined by the experimental measurements. First, the end point of the curve must correspond to the measured values of impact stress and permanent strain at the impact end of the bar; that is, the curve must terminate on the stress-plastic strain measurement relation shown in Fig. 5. This condition may be expressed in terms of the wave velocity function

$$c^*(\epsilon) = \sqrt{\frac{1}{\rho} \frac{d\sigma(\epsilon)}{d\epsilon}} \quad (4)$$

associated with that particular stress-strain curve by means of the relation

$$\sigma_1 = \int_0^{\epsilon_1} \rho \{c^*(\epsilon)\}^2 d\epsilon \quad (5)$$

where $\sigma(\epsilon)$ denotes the desired stress-strain relation. Second, the particle velocity due to the impact as given by

$$v_1 = \int_0^{\epsilon_1} C^*(\epsilon) d\epsilon \quad (6)$$

must be equal to the particle velocity for that particular impact stress as determined experimentally. Third, for strains in the elastic region, the wave velocity must be equal to the normal velocity of elastic waves in long rods; namely,

$$C^*(\epsilon) = \sqrt{\frac{E}{\rho}} \quad \text{for } \epsilon \leq \epsilon_0 \quad (7)$$

where ϵ_0 is the elastic limit strain, and E is Young's modulus for the material. Finally, the stress-strain relation must be such that by constructing a suitable Lagrange diagram based upon it, curves of permanent strain distribution in the specimen may be obtained which agree with the experimental strain distribution curves. It is not possible to express this last condition in closed mathematical form. Hence, it will not be used explicitly, but it will be shown later that the stress-strain relations chosen lead to an improved agreement between predicted and measured strain distributions, particularly in regard to the distance traveled by the maximum strain, ϵ_1 , during the impact.

Thus, all of the explicit conditions to be satisfied by each member of the desired family of stress-strain relations have been expressed in terms of the wave velocity as a function of strain, $C^*(\epsilon)$, as given by Equations 5, 6, and 7 above. Once $C^*(\epsilon)$ is determined, the corresponding stress-strain relation may be readily determined by the use of Equation 5 with arbitrary values of σ and ϵ replacing σ_1 and ϵ_1 . Of course, these three conditions are insufficient to determine $C^*(\epsilon)$ unambiguously; hence, the form of the function must be chosen somewhat arbitrarily. The assumed form of the wave velocity function is

$$\begin{aligned} C^*(\epsilon) &= C_0 \quad \text{for } \epsilon \leq \epsilon_0 \\ C^*(\epsilon) &= C(\epsilon) + \Delta C(\epsilon) \quad \text{for } \epsilon, \geq \epsilon \geq \epsilon_0. \end{aligned} \quad (8)$$

$$\text{with } \Delta C(\epsilon) = a(\epsilon - \epsilon_0)$$

where $C_0 = \sqrt{\frac{E}{\rho}}$ is the elastic wave velocity,

$C(\epsilon) = \sqrt{\frac{1}{\rho} \frac{d\sigma_1}{d\epsilon_1}}$ is the wave velocity corresponding to the experimental stress-plastic strain measurement curve shown in Fig. 7,

ϵ_0 is an undetermined constant representing the elastic limit strain on the desired stress-strain curve, and

a is a second undetermined constant.

Both ϵ_0 and a depend upon the final strain, ϵ_1 , corresponding to each individual member of the family of stress-strain curves to be determined.

Substitution of the assumed form of the wave velocity as given by Equation 8 into Equations 5 and 6 yields two relations in the unknowns ϵ_0 and a . A trial and error solution was used to determine the values of a and ϵ_0 corresponding to final strains of 2.0, 3.5, and 5.0 per cent. The stress-strain relations are then computed from Equation 5. These are shown in Fig. 21. The stress-strain relations determined from stress-velocity measurements and from stress-plastic strain measurements are shown for comparison.

The family of stress-strain relations deduced in the above manner may now be compared with experimental results which are independent of the data upon which the deduction is based; namely, from any particular member of the family of stress-strain relations, the distance which the maximum strain, ϵ_1 , should propagate along the specimen may be predicted by constructing a suitable Lagrange diagram based upon that stress-strain relation. This predicted distance of propagation may then be compared with the corresponding experimental value as determined from the measurements of plastic strain distribution. The required Lagrange diagrams need only be partially constructed to determine the desired propagation distance, and this reduces the labor involved by a large factor. The above procedure has been carried out for the values of the maximum impact strain, ϵ_1 , of 2.0, 3.5, and 5.0 per cent. The partial Lagrange diagram for the case $\epsilon_1 = 5$ per cent is shown in Fig. 22. The results of all these computations are given in Table III, together with the corresponding propagation distances predicted from the original Lagrange diagram deduced from stress-velocity measurements and the experimental distances of propagation for the same values of ϵ_1 . These results show that the propagation distances computed from the stress-strain relations which depend upon the final strain compare more favorably with the measured values than the distances computed from stress-velocity measurements.

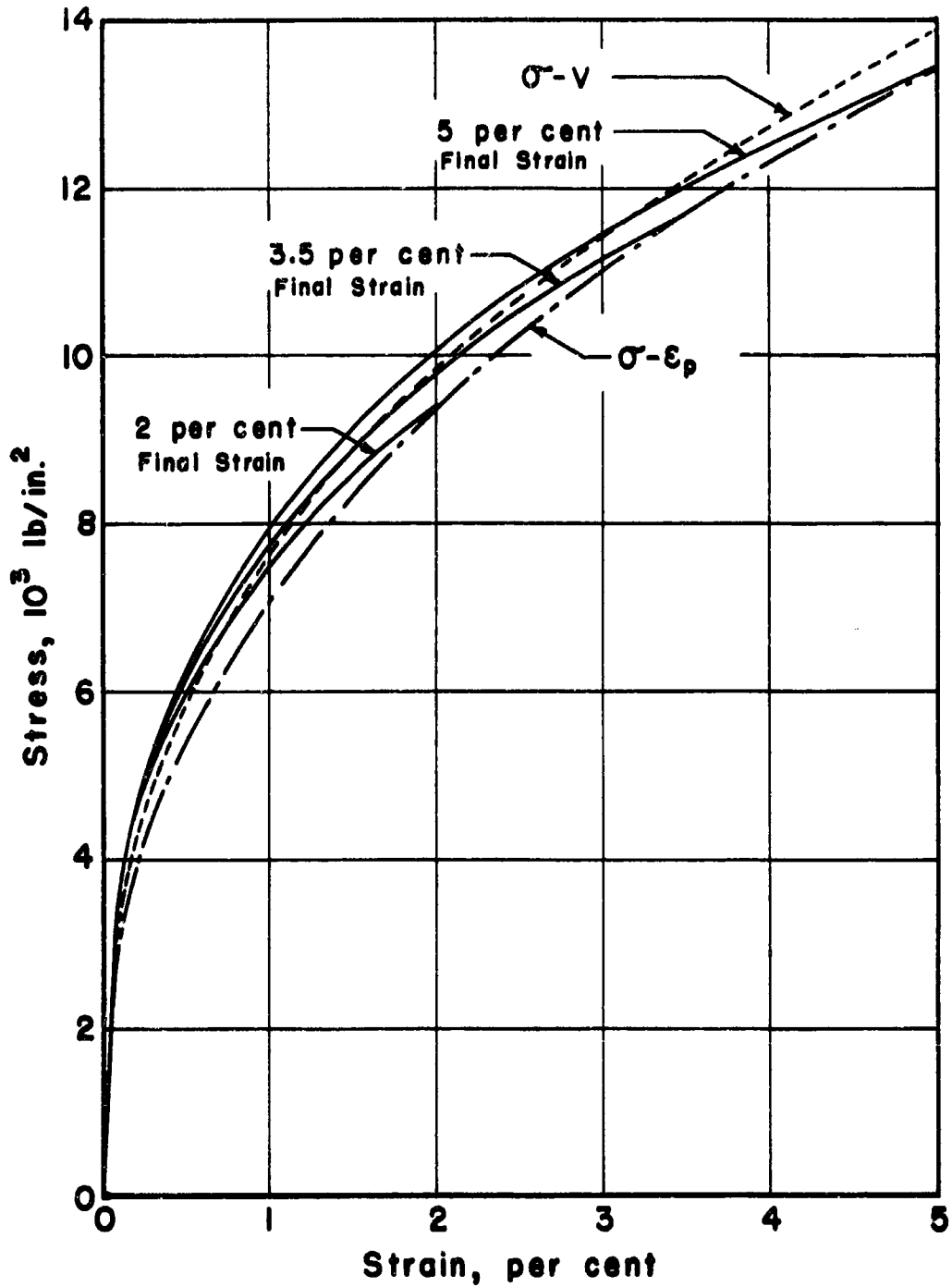


Fig. 21 Derived Dynamic Stress-Strain Curves Which Depend Upon the Final Strain in Relation to Curves Based on $\sigma - v$ and $\sigma - \epsilon_p$ Measurements

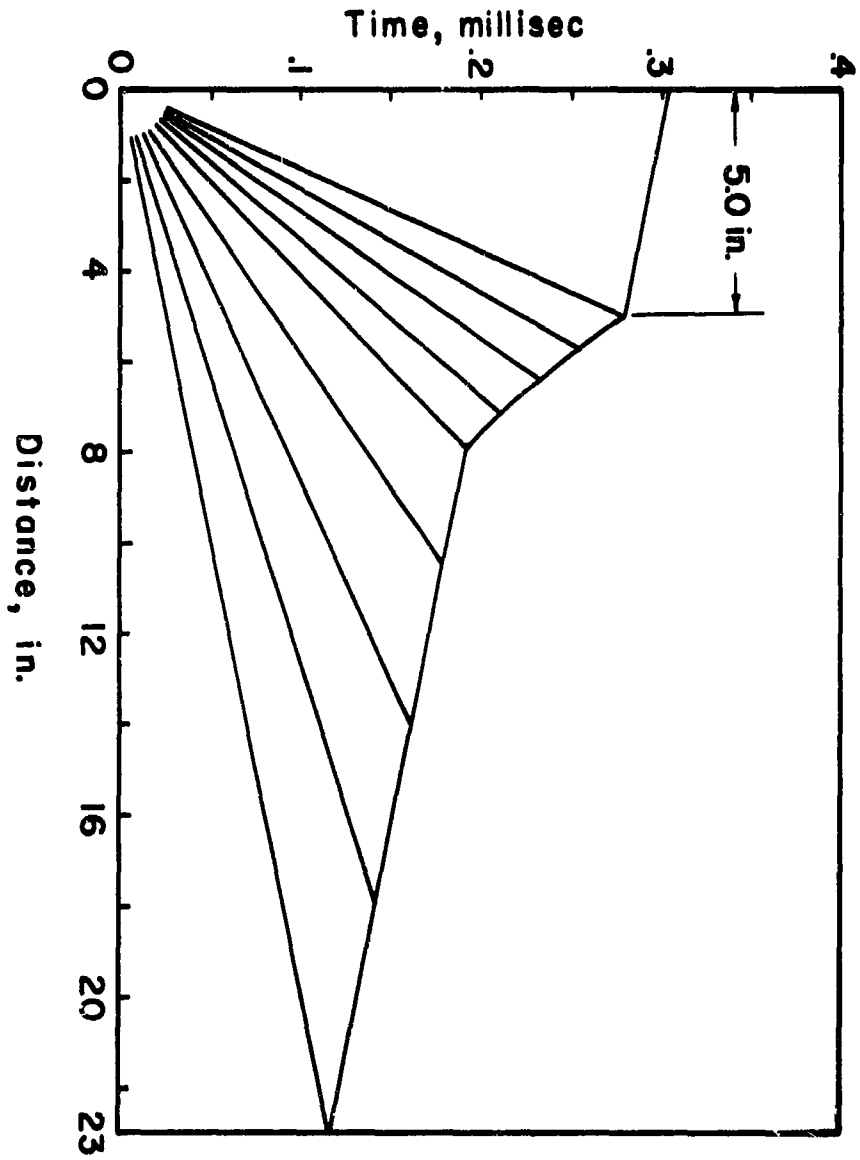


Fig. 22 Lagrange Diagram for Stress-Strain Relation up to 5 per cent Strain

Table III
 PROPAGATION DISTANCES OF MAXIMUM STRAINS

Maximum Strain Per Cent	From Plastic Strain Distribution Measurements		A	B
	In.		In.	In.
2.0	5.0		7.0	5.9
3.5	4.0		6.2	5.3
5.0	5.0		5.8	5.0

A - From Lagrange diagram deduced from stress-velocity measurements.

B - From Lagrange diagrams deduced from stress-strain relations which depend upon the final strain, ϵ_1 .

The stress-strain relations which depend upon the final strain, shown in Fig. 21, are consistent with the generally accepted idea that stress-strain relations are progressively raised as the rate of loading is increased. In this present case, the rate of loading increases as the impact velocity (and corresponding impact stress, σ_1 , and final strain ϵ_1) is increased. The reason for this is twofold. First, the rise time of the stress at the impact surface decreases as the impact velocity is increased, because the time required for the end surface of the specimen to deform into conformity with the spherical end surface of the anvil bar decreases for increasing impact velocity. Hence, the mean loading rate given by the ratio of the impact stress to the stress rise time increases with increasing impact velocity.

The behavior of a specimen subjected to a given impact cannot (strictly speaking) be completely described on the basis of the appropriate member of the family of stress-strain relations if it is assumed, as indicated above, that the differences between the members of this family of curves are due to differences in loading rates. This is simply due to the fact that in such an impact the loading rate varies rather widely with position along the specimen and with time at any given position. In general, the loading rates decrease with increasing distance from the impact surface. Thus, since different stress-strain relations correspond to each loading rate, no single stress-strain relation can be employed, strictly speaking, to describe the behavior of the entire specimen. It may be noted that the family of stress-strain relations determined

above were deduced from experimental data measured at the impacted end of the specimens. Hence, these stress-strain relations correspond to the highest loading rates present in the specimens. The stress rise times at the impact surface in these experiments are estimated to be in the range of 2 to 20 microsec, with the longer times corresponding to lower impact velocities. Thus, the mean loading rates at the impact surface were probably in the range 2×10^8 to 7×10^9 lb/in.² per sec.

A complete description of the wave propagation effects under impact loading in a material exhibiting time-dependent mechanical properties must be based upon a complete stress-strain-time relation for that material. One attempt at such a treatment has been given by Malvern (19). Unfortunately, the particular form of the time dependence of the stress-strain properties assumed by Malvern does not seem to be capable of predicting behavior which is consistent with the results of impact experiments. The problem of finding functional relationships between stress, strain, and time which provide for agreement between theory and experiment and are at the same time mathematically feasible to use is probably very difficult.

Fortunately, the complexities and difficulties of theoretical treatment just discussed are concerned with effects of rather minor magnitude in many materials, as judged from experimental investigations. Thus, the results of the present experiments indicate that the behavior of annealed 2S aluminum under impact conditions may be predicted with good accuracy, using a single time-independent dynamic stress-strain relation. In this case, for example, a stress-strain relation which is an average between the curve deduced from stress-velocity measurements and the curve deduced from stress-plastic strain measurements could be used to predict plastic wave propagation phenomena with good accuracy.

Qualitatively similar behavior under impact loading is to be expected for materials which are similar to 2S aluminum in other respects. Thus, pure metals and solid-solution alloys which exhibit the face-centered cubic crystal structure may be expected to behave in the same general manner. Examples of such materials are copper and austenitic stainless steel. However, low-carbon steel and probably other body-centered cubic metals behave quite differently under suddenly applied loads (15, 20).

During the preparation of this report, a report of a similar investigation by J. D. Campbell (21) was published. Campbell's experiments differed from those reported here in that repeated impacts on the same specimen were employed, and the impact velocities used did not cover nearly as wide a range as in the present investigation. Nevertheless, Campbell obtains a raised dynamic stress-strain relation for an annealed aluminum alloy for strains up to 0.6 per cent which is very similar to the results reported in this report. Campbell's data and analysis are not sufficient to show that the dynamic stress-strain relation varies slightly with impact stress.

SUMMARY

The results of this investigation show that the behavior of annealed 2S aluminum under conditions of impact loading into the plastic strain range can be represented to a good approximation by a single dynamic stress-strain relation. This dynamic stress-strain relation lies above the static stress-strain curve. The excess of dynamic stress over the static values increases progressively with strain, reaching about 20 per cent of the static stress at a strain of 4.5 per cent.

However, the results also show that higher order effects cannot be correlated with such a single dynamic stress-strain relation. A detailed analysis of the experimental measurements by means of the von Kármán theory of propagation of plastic strains in long rods indicates that the behavior of the material near the impact surface may be described by a family of stress-strain relations. Each member of this family of curves corresponds to a given impact stress, and the curves are arranged consecutively in order of increasing impact stress. All of these curves lie within a narrow region in the stress-strain plane.

APPENDIX

The present theory of the propagation of longitudinal waves of plastic deformation in long, thin bars was developed by von Kármán (13, 14). The methods of integration and graphical solutions for problems of strain propagation were developed by von Kármán, Bohnenblust, Hyers, and Charyk (16, 17). Since these reports are not readily available, a summary of the graphical solution used in this investigation will be given.

Let the stress-strain relation for the material be given by a function of the form $\sigma = \sigma(\epsilon)$ where σ is the stress and ϵ is the strain. This relation holds for the first deformation of the material beyond the elastic limit. If the load is decreased, the stress and strain decrease according to Hooke's law.

Consider a long bar of the material in which one end of the bar is suddenly put into motion by longitudinal impact. The characteristic parameters which define the state of strain and motion of an element in the bar are the following:

$$\epsilon = \frac{\partial u}{\partial x} = \text{strain}$$

$$\sigma = \text{stress}$$

$$v = \frac{\partial u}{\partial t} = \text{particle velocity}$$

where x is the distance along the bar, and

u is the longitudinal displacement of a cross section.

The equation of motion of a small element of the rod, neglecting the kinetic energy and shear stresses associated with the radial motion of the bar, is given by

$$\rho \frac{\partial v}{\partial t} = \frac{\partial \sigma}{\partial x}$$

where ρ is the mass density of the material. Using the relation for the velocity of propagation of a plastic strain as shown by von Kármán (13),

$$c = \sqrt{\frac{d\sigma}{d\epsilon} / \rho} ,$$

the equation of motion becomes

$$\frac{\partial v}{\partial t} = c^2 \frac{\partial \epsilon}{\partial x} . \quad (9)$$

On the other hand, from the relations $v = \frac{\partial u}{\partial t}$ and $\epsilon = \frac{\partial u}{\partial x}$, it follows that

$$\frac{\partial v}{\partial x} = \frac{\partial \epsilon}{\partial t} . \quad (10)$$

By using a transformation of variables, the strain, ϵ , and the particle velocity, v , are introduced as independent variables. Then Equations 9 and 10 take the form

$$\begin{aligned} \frac{\partial x}{\partial \epsilon} &= c^2 \frac{\partial t}{\partial v} \\ \frac{\partial t}{\partial \epsilon} &= \frac{\partial x}{\partial v} . \end{aligned} \quad (11)$$

The equations become more symmetrical by introduction of the function $\phi = \int c d\epsilon$. The equations become

$$\begin{aligned} \frac{\partial x}{\partial \phi} &= c \frac{\partial t}{\partial v} \\ \frac{\partial x}{\partial v} &= c \frac{\partial t}{\partial \phi} . \end{aligned} \quad (12)$$

The process of propagation can be represented in a Lagrangean plane with x and t as coordinates, and a velocity plane with v and ϕ as coordinates. The Equations 12 have fixed characteristics in the v, ϕ plane. They are given by the family of straight lines $v - \phi = \text{constant}$ and $v + \phi = \text{constant}$. The Lagrange diagram serves as a means of representing the values of stress, particle velocity, and strain at any time and position along the specimen. The details of the construction of the Lagrange diagram shown in Fig. 9 are given below.

The relations c vs. ϵ , ϕ vs. ϵ , ϕ vs. c , and ϕ vs. σ are plotted from the engineering stress-strain curve of the material. Compression stresses will be taken to be positive, and particle velocity will be taken to be positive when the material moves toward the right

of the Lagrange diagram shown in Fig. 9. It is assumed that the behavior of the material is characterized by the given stress-strain relation for increasing or constant values of strain and that Hooke's law holds for decreasing strain.

The Lagrange diagram consists of two regions: the plastic region and the hysteresis region. In the plastic region, the quantity $v + \phi$ is constant along the characteristic of slope $1/c$, while the quantity $v - \phi$ is constant along the characteristic of slope $-1/c$. The plastic region is also described by the differential equations $\frac{\partial \sigma}{\partial x} = -\rho \frac{\partial v}{\partial t}$ and $\frac{\partial \sigma}{\partial t} = -\rho c^2 \frac{\partial v}{\partial x}$. Similarly, in the hysteresis region, the quantity $v + \frac{\sigma}{c_0}$ is constant along the characteristic of slope $1/c_0$ while the quantity $v - \frac{\sigma}{c_0}$ is constant along the characteristic $-1/c_0$. The hysteresis region is also described by the differential equations $\frac{\partial \sigma}{\partial x} = -\rho \frac{\partial v}{\partial t}$ and $\frac{\partial \sigma}{\partial t} = -\rho c_0^2 \frac{\partial v}{\partial x}$. The construction of the Lagrange diagram consists in determining the characteristics in the plastic and hysteresis regions. The determination of the boundary between the plastic and hysteresis regions allows the characteristics in both regions to be constructed.

The construction of the Lagrange diagram is simplified if it is assumed that the specimen is initially at rest and a moving anvil bar strikes the end of the specimen. At time, $t = 0$, the anvil bar moving with a velocity, V_0 , strikes the specimen, and a series of plastic strains are propagated toward the free end of the specimen. The particle velocity at the end of the specimen is equal to the value of ϕ corresponding to the stress at the impact end. The values of σ and v are determined from the relation given by Equation 2 and the ϕ vs. σ curve. The propagation velocity of the plastic strains vary from c_0 for the "elastic front" to c_1 for the "plastic front" where c_1 is determined from the ϕ vs. c curve.

At time, $t = l/c_0$, where l is equal to the specimen length, the elastic wave reaches the free end of the specimen and reflects as an unloading "shock wave." This "shock wave" is stopped at a point, 2, which is determined from the equation

$$\frac{2 \sigma_1}{\rho c_0} = v_2 - \frac{\sigma_2}{\rho c_0} \quad (13)$$

where σ_1 is the proportional limit of the material,

σ_2 is the stress at the point 2, and

v_2 is the particle velocity at the point 2.

Since σ and v are known along each characteristic, the point 2 can be readily determined.

The Lagrange diagram now consists of two regions: the plastic region below the unloading wave and the hysteresis region above the unloading wave. The stress and particle velocity are discontinuous across the boundary since the unloading "shock wave" is of finite magnitude. The remaining portion of the boundary between the plastic and hysteresis regions is considerably more complicated than the boundary obtained from the unloading "shock wave." The stress and particle velocity are continuous across the remaining portion of the boundary between the plastic and hysteresis regions, but in general their partial derivatives are not continuous. Using the differential equation of motion and expressing the fact that σ and v are continuous across the boundary, the following equation is obtained:

$$\left[2 \left(\frac{dx}{dt} \right)^2 - (c^2 + c_0^2) \right] \left[\left(\frac{\partial v}{\partial x} \right)_h - \left(\frac{\partial v}{\partial x} \right)_p \right] = (c_0^2 - c^2) \left[\left(\frac{\partial v}{\partial x} \right)_h + \left(\frac{\partial v}{\partial x} \right)_p \right] \quad (14)$$

where $\left(\frac{\partial v}{\partial x} \right)_h$ denotes the value of the partial derivative on the hysteresis side,

$\left(\frac{\partial v}{\partial x} \right)_p$ denotes the value of the partial derivative on the plastic side, and

$\frac{dx}{dt}$ is the slope of the boundary.

The method of solution of the boundary is dictated by this equation.

In the solution of the boundary on the right side of the Lagrange diagram shown in Fig. 9, the plastic region is to the left of the boundary, and the hysteresis region to the right. The boundary is assumed to be constructed up to a cross section, $t = \text{constant}$, passing through a point F of the boundary (see Fig. 23). A characteristic, a , is chosen arbitrarily in the hysteresis region, and the problem is to determine the end point, P, of a where a intersects the plastic region. The boundary is given by the line FP. The plastic and hysteresis regions are then constructed

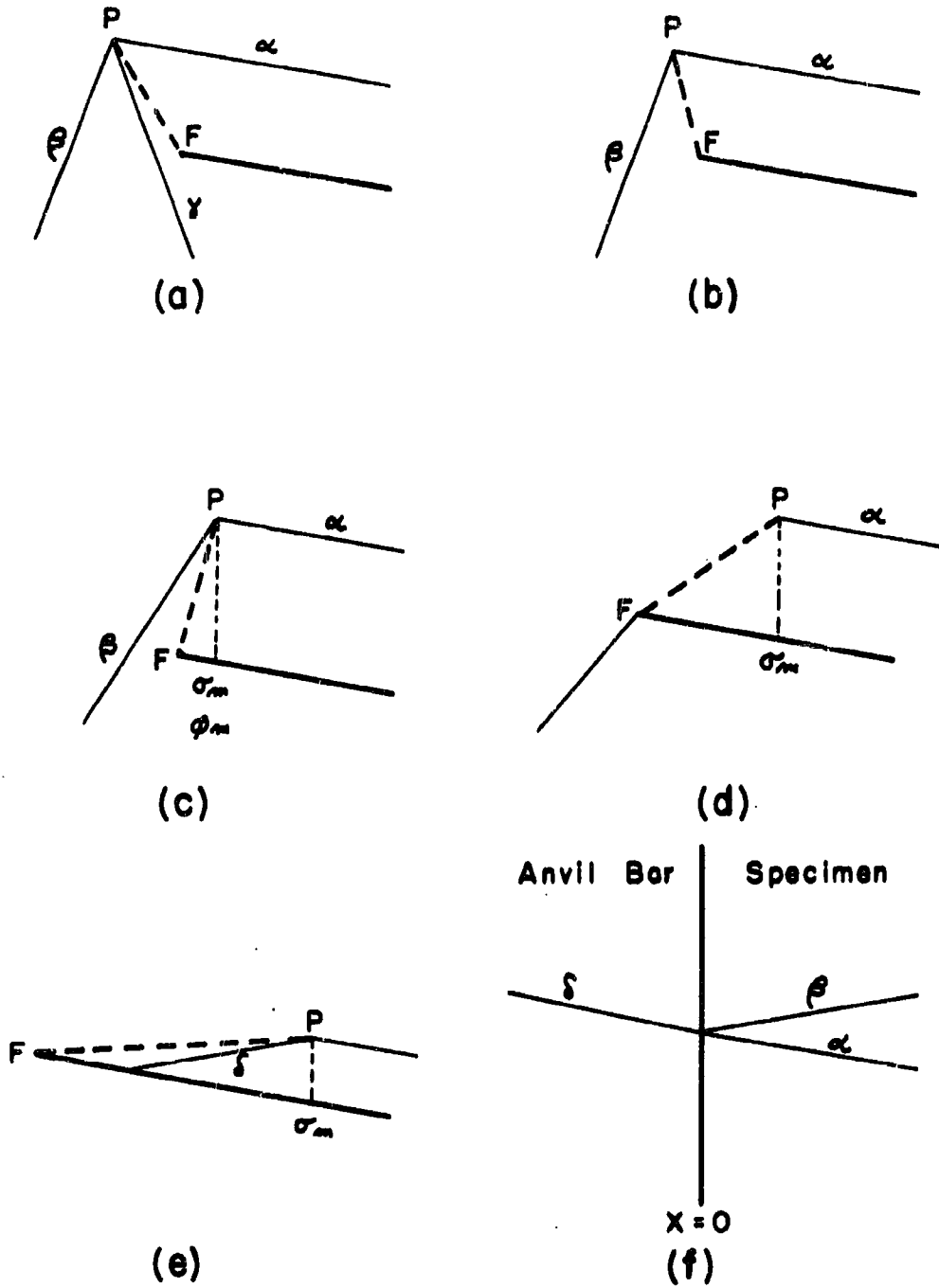


Fig. 23 Steps Illustrating Construction of Lagrange Diagram

up to the new cross section passing through P. The unknown point, P, lies in one of five regions. A different method, determined by Equation 14, applies in each region, but in all cases the value of $v - \frac{\sigma}{\rho c_0} = k_1$ is known along the characteristic α . The five regions in which P may lie are determined by the following conditions.

Region A (Fig. 23a) $-\frac{1}{c} < \frac{\Delta t}{\Delta x} < -\frac{1}{c_0}$

Choose a characteristic α along which $v - \frac{\sigma}{\rho c_0} = k_1$

$$\text{Along } \beta \quad v + \phi = k_2 \quad (15)$$

$$\text{Along } \delta \quad v - \phi = k_3 \quad (16)$$

The value of v and ϕ at P can be computed from Equations 15 and 16. The value of σ corresponding to ϕ is obtained from the $\sigma - \phi$ curve. These values of v and σ must be compatible with α .

Region B (Fig. 23b) $\frac{\Delta t}{\Delta x} < -\frac{1}{c}$

In this case, $\frac{\partial \sigma}{\partial t} = \frac{\partial v}{\partial x} = 0$ along the boundary from Equation 14. This implies that $\frac{\sigma}{\rho c_0} + \frac{v}{c_0} \left(\frac{dx}{dt} \right)$ is constant along the boundary and, therefore, equal to its value at F.

Choose a characteristic α along which $v - \frac{\sigma}{\rho c_0} = k_1$.

$$\text{Along the boundary } \frac{\sigma}{\rho c_0} + \frac{v}{c_0} \left(\frac{dx}{dt} \right) = k_3 \quad (17)$$

$$\text{Along } \beta \quad v + \phi = k_2 \quad (18)$$

The constant value of $v + \phi = k_2$ along the characteristic of slope $1/c$ which abuts at P must be compatible with α and Equation 17.

Region C (Fig. 23c) $\frac{\Delta t}{\Delta x} > \frac{1}{c}$

Choose a characteristic α along which $v - \frac{\sigma}{\rho c_0} = k_1$.

$$\text{Along } \beta \quad v + \phi = k_2 \quad (19)$$

At P, $\sigma = \sigma_{\max}$ and $\phi = \phi_{\max}$ determined from the previous boundary. The point P is determined from

$$\frac{\sigma_{\max}}{\rho c_0} + \phi_{\max} = k_2 - k_1.$$

Region D (Fig. 23d) $1/c_0 < \frac{\Delta t}{\Delta x} < \frac{1}{c}$

In this case $\frac{\partial \sigma}{\partial t} = \frac{\partial v}{\partial x} = 0$ along the boundary from Equation 14.

This implies that $\frac{\sigma}{\rho c_0} + \frac{v}{c_0} \left(\frac{dx}{dt}\right)$ is constant along the boundary and, therefore, equal to its value at F.

Choose a characteristic d along which $v - \frac{\sigma}{\rho c_0} = k_1$

$$\text{Along the boundary } \frac{\sigma}{\rho c_0} + \frac{v}{c_0} \left(\frac{dx}{dt}\right) = k_3 \quad (20)$$

$$\text{At P } \sigma = \sigma_{\max}.$$

The value of σ_{\max} at P must be compatible with d and Equation 20.

Region E (Fig. 23e)

Choose a characteristic d along which $v - \frac{\sigma}{\rho c_0} = k_1$.

$$\text{Along } \delta \quad v + \frac{\sigma}{\rho c_0} = k_4 \quad (21)$$

$$\text{At P } \sigma = \sigma_{\max}.$$

The following relation must hold

$$\frac{2 \sigma_{\max}}{\rho c_0} = k_2 - k_1.$$

Finally, having found point, P, the Lagrange diagram is extended up to the line, $t = \text{constant}$, passing through P. At P, σ , v , and ϕ have been determined. The values of $v \pm \phi$ and $v \pm \frac{\sigma}{\rho c_0}$ are known along the characteristics starting from P with the slopes $\pm 1/c$ and $\pm 1/c_0$ respectively. The characteristics are then plotted in the plastic and hysteresis regions.

The boundary on the left side of the Lagrange diagram shown in Fig. 9 is constructed in a similar manner. In this case, the plastic region

is to the right of the boundary and the hysteresis region to the left of the boundary. A condition equivalent to Region A for the right boundary is used to determine the left boundary.

The hysteresis region on the left side of the Lagrange diagram is extended to the interface, $x = 0$, and an additional computation must be made to determine the characteristics in the anvil bar and specimen. The characteristics shown in Fig. 23 satisfy the following conditions:

$$\text{Along } \alpha \quad v - \frac{\sigma}{\rho c_0} = k_1 \quad (22)$$

$$\text{Along } \beta \quad v + \frac{\sigma}{\rho c_0} = k_2 \quad (23)$$

$$\text{Along } \delta \quad v - \frac{\sigma}{\rho c_0} = k_3 \quad (24)$$

where $\overline{\rho c_0}$ is the acoustic impedance of the anvil bar, and

ρc_0 is the acoustic impedance of the specimen.

In all cases, the value of $v - \frac{\sigma}{\rho c_0} = k_1$ is known along the characteristic α . Since the anvil bar remains elastic, k_3 is given by

$$k_3 = 2v - V_0 \quad (25)$$

where V_0 is the velocity of impact. The value of k_2 is determined from Equations 22, 23, 24, and 25, giving

$$k_2 = \frac{2V_0 \gamma}{\gamma + 1} - k_1 \left(\frac{\gamma - 1}{\gamma + 1} \right) \quad (26)$$

where γ is equal to $\frac{\overline{\rho c_0}}{\rho c_0}$. The stress and particle velocity at the interface are given by

$$\sigma = \frac{(k_2 - k_1)}{2} \rho c_0 \quad (27)$$

$$v = \frac{k_1 + k_2}{2} \quad (28)$$

The values of σ , v , and ϕ are tabulated for each characteristic intersection and determined boundary point. The values between these intersections and points are determined by linear interpolation. Thus, the values of σ , v , and ϕ for any time or position along the specimen can be determined directly from the Lagrange diagram.

The plastic strain distribution in the specimen after impact is obtained from the Lagrange diagram. The highest value of ϕ reached at various positions along the bar is determined at the plastic-hysteresis boundary, and translated into ϵ values from the $\phi - \epsilon$ curve. The strains are then corrected for elastic recovery upon removal of load.

The strain-time relation at any position along the specimen is similarly obtained from the Lagrange diagram. The values of ϵ along a line, $x = \text{constant}$, are determined by reading from the $\phi - \epsilon$ curve, the values of ϵ corresponding to the values of ϕ .

The stress-time relation at the interface between the anvil bar and specimen is determined from the Lagrange diagram along the line, $x = 0$.

REFERENCES

- (1) H. C. Mann, "High Velocity Tension Impact Tests," Proceedings of the American Society for Testing Materials, Vol. 36, Part II, 1936, p. 85.
- (2) D. S. Clark and G. Dätwyler, "Stress-Strain Relations Under Tension Impact Loading," Proceedings of the American Society for Testing Materials, Vol. 38, Part II, 1938, p. 98.
- (3) M. Manjoine and A. Nadai, "High Speed Tension Tests at Elevated Temperatures," Proceedings of the American Society for Testing Materials, Vol. 40, 1940, p. 822; Journal of Applied Mechanics, Trans. ASME, Vol. 8, No. 2, 1941, p. A-77.
- (4) D. S. Clark, "The Influence of Impact Velocity on the Tensile Characteristics of Some Aircraft Metals and Alloys," National Advisory Committee for Aeronautics, Technical Note No. 868, October, 1942.
- (5) P. E. Duwez and D. S. Clark, "An Experimental Study of the Propagation of Plastic Deformation Under Conditions of Longitudinal Impact," Proceedings of the American Society for Testing Materials, Vol. 47, 1947, p. 502.
- (6) D. S. Clark and P. E. Duwez, "Discussion on the Forces Acting in Tension Impact Tests of Materials," Journal of Applied Mechanics, Trans. ASME, Vol. 15, No. 3, 1948, p. A-243.
- (7) G. I. Taylor, "The Use of Flat Ended Projectiles for Determining Dynamic Yield Stress. Part I-Theoretical Considerations," Proceedings of the Royal Society, London, Vol. 194, No. A 1038, 1948, p. 289.
- (8) A. C. Whiffin, "The Use of Flat Ended Projectile for Determining Dynamic Yield Stress. Part II-Tests on Various Metallic Materials," Proceedings of the Royal Society, London, Vol. 194, No. A 1038, 1948, p. 300.
- (9) E. T. Habib, "A Method of Making High-Speed Compression Tests on Small Copper Cylinders," Journal of Applied Mechanics, Trans. ASME, Vol. 15, 1948, p. 248.
- (10) D. S. Clark and D. S. Wood, "The Tensile Impact Properties of Some Metals and Alloys," Transactions of the American Society for Metals, Vol. 42, 1950, p. 45.
- (11) E. H. Lee and H. Wolf, "Plastic-Wave Propagation Effects in High-Speed Testing," Journal of Applied Mechanics, Trans. ASME, Vol. 18, No. 4, 1951, p. 379.

- (12) H. Kolsky, "An Investigation of the Mechanical Properties of Materials at Very High Rates of Loading," Proceedings of the Physical Society, London, Vol. 62, 1949, p. 176.
- (13) Th. von Kármán, "On the Propagation of Plastic Deformation in Solids," NDRC Report No. A-29 (OSRD No. 365), 1942.
- (14) Th. von Kármán and P. E. Duwez, "The Propagation of Plastic Deformation in Solids," Journal of Applied Physics, Vol. 21, No. 10, 1950, p. 987.
- (15) J. E. Johnson, D. S. Wood, and D. S. Clark, "Delayed Yielding in Annealed Low-Carbon Steel Under Compression Impact," Fifth Technical Report under Office of Naval Research, Contract N6onr-24418, March 1952; also submitted to American Society for Testing Materials, December 1952.
- (16) Th. von Kármán, H. F. Bohnenblust, and D. H. Hyers, "The Propagation of Plastic Waves in Tension Specimens of Finite Length. Theory and Methods of Integration," NDRC Report No. A-103 (OSRD No. 946), 1942.
- (17) H. F. Bohnenblust, J. V. Charyk, and D. H. Hyers, "Graphical Solutions for Problems of Strain Propagation in Tension," NDRC Report No. A-131 (OSRD No. 1204), 1942.
- (18) E. Jones and K. R. Maslan, "The Physical Characteristics of Wire Resistance Strain Gages," Royal Aircraft Establishment, Farnborough, England.
- (19) L. E. Malvern, "The Propagation of Longitudinal Waves of Plastic Deformation in a Bar of Material Exhibiting a Strain-Rate Effect," Journal of Applied Mechanics, Trans. ASME, Vol. 18, No. 2, 1951, p. 203.
- (20) D. S. Clark and D. S. Wood, "The Time Delay for the Initiation of Plastic Deformation at Rapidly Applied Constant Stress," Proceedings of the American Society for Testing Materials, Vol. 49, 1949, p. 717.
- (21) J. D. Campbell, "An Investigation of the Plastic Behavior of Metal Rods Subjected to Longitudinal Impact," Journal of the Mechanics and Physics of Solids, Vol. 1, No. 2, 1953, p. 113.